Helsinki University of Technology Communications Laboratory Technical Report T56
Teknillinen korkeakoulu Tietoliikennelaboratorio Raportti T56
Espoo 2007

FIBER-OPTIC CODE DIVISION MULTIPLE ACCESS:

MULTI-CLASS OPTICAL ORTHOGONAL CODES, OPTICAL POWER CONTROL, AND POLARIZATION ENCODING

Naser G. Tarhuni

TEKNILLINEN KORKEAKOULU
TEKNISKA HÖGSKOLAN
HELSINKI UNIVERSITY OF TECHNOLOGY
TECHNISCHE UNIVERSITÄT HELSINKI
UNIVERSITE DE TECHNOLOGIE D'HELSINKI

Helsinki University of Technology Communications Laboratory Technical Report T56
Teknillinen korkeakoulu Tietoliikennelaboratorio Raportti T56
Espoo 2007

FIBER-OPTIC CODE DIVISION MULTIPLE ACCESS:

MULTI-CLASS OPTICAL ORTHOGONAL CODES, OPTICAL POWER CONTROL, AND POLARIZATION ENCODING

Naser G. Tarhuni

Dissertation for the degree of Doctor of Science in Technology to be presented with due permission for public examination and debate in Auditorium S4 at Helsinki University of Technology (Espoo, Finland) on the 26th April, 2007, at 12 o'clock noon.

Helsinki University of Technology
Department of Electrical and Communications Engineering
Communications Laboratory

Teknillinen korkeakoulu
Sähkö- ja tietoliikennetekniikan osasto
Tietoliikennelaboratorio

Distributor:
Helsinki University of Technology
Communications Laboratory
P.O. Box 3000
FIN-02015 HUT
Tel. +358-9-451 2366
Fax +358-9-451 2345

ISBN 978-951-22-8723-9 (paper)
ISBN 978-951-22-8724-6 (electronic)
ISSN 0356-5087
URL: http://lib.tkk.fi/Diss/2007/isbn9789512287246

Multiprint Oy/Otamedia
Espoo 2007

ABSTRACT OF DOCTORAL DISSERTATION	HELSINKI UNIVERSITY OF TECHNOLOGY P.O. BOX 1000, FI-02015 TKK http://www.tkk.fi

Author Naser G. Tarhuni

Name of the dissertation
Fiber-Optic Code Division Multiple Access:
Multi-Class Optical Orthogonal Codes, Optical Power Control, and Polarization Encoding

Manuscript submitted 18.12.2006	Manuscript revised 2.3.2007
Date of the defence April 26, 2007	
☐ Monograph	☒ Article dissertation (summary + original articles)

Department Electrical and Communications Engineering
Laboratory Communications Laboratory
Field of research Communications Engineering
Opponent(s) Dr. Mohammed M. Banat
Supervisor Adj. Prof. Timo Korhonen

Abstract

Ever since the mid- 1980s when the single-mode fiber-optic media were believed to become the main highways of future telecommunications networks for transporting high-volume high-quality multipurpose information, the need for all-optical multi-access networking became important. An all-optical multi-access network is a collection of multiple nodes where the interconnection among various nodes is via single- or multi-mode fiber optics and for which they perform all their essential signal processing requirements such as switching, add-drop, multiplexing/demultiplexing and amplification in the optical domain. Optical CDMA networking is one possible technique that allows multiple users in local area networks to access the same fiber channel asynchronously with no delay or scheduling.

Optical CDMA networks are not without their own problems. Search for codes suitable to the optical domain is one of the important topics addressed in the literature on optical CDMA. Existing codes developed in the late 80's are limited to single class traffic or can support multiclass traffic but with restrictions on code lengths and weights. Also the number of generated codes is severely limited due to orthogonality issues. In this thesis, we pay particular attention to propose new codes that can support multiclass traffic with arbitrary code weights and lengths. Therefore, data sources with varying traffic demands can be accommodated by optical CDMA networks using the proposed codes. We also present a simple generation technique for the proposed multiclass codes and analyze their performance. The number of users supported by the proposed multiclass codes will be limited since it is an extension of existing code designs with such limitation. We then propose the use of polarization dimension in order to double the number of supported users.

On the other hand, incoherent optical CDMA systems are considered as positive systems meaning that only unipolar codes can be considered for such systems. Therefore, multiple access interference will be quite high in optical CDMA due to the nature of incoherent power detection. Reducing the effect of the interference on the performance of optical CDMA is an important topic. We propose the use of power control to decrease the effects of interference in optical star networks in which users' fiber lengths and data rates are not equal. We consider the case of optically amplified network with amplifier noise as the main source. We then elaborate by considering the nonlinearity in the photodetection process and propose the use of an iterative algorithm to find the solution of the non-linear optical power control problem.

Finally, we propose an optical CDMA system based on polarization encoding. Since the encoding is performed in the spatial domain, therefore, positive and negative levels can be realized. This approach leads to increasing the number of supported users of optical CDMA by the use of known codes, such as Gold and Hadamard codes, with enhanced performance.

Keywords Optical CDMA, Optical Orthogonal Codes, Optical Power Control, Polarization Shift Keying

ISBN (printed) 978-951-22-8723-9	ISSN (printed) 0356-5087
ISBN (pdf) 978-951-22-8724-6	ISSN (pdf)
Language English	Number of pages 63+app. 61
Publisher Helsinki University of Technology, Communications Laboratory	
Print distribution Helsinki University of Technology, Communications Laboratory	
☒ The dissertation can be read at http://lib.tkk.fi/Diss/2007/isbn9789512287246	

Preface

First of all, thanks should be forwarded to God, the most gracious, the most merciful, Who guides me in every step I take.

The work in this thesis was carried out at the Communications Laboratory of the Helsinki University of Technology. I take this opportunity to express my sincere gratitude to my supervisor Prof. Timo Korhonen for providing me with the opportunity to do this work. Moreover, his support, guidance and proofreading of the thesis is immensely appreciated. The administrative and support staff of the Communications Laboratory also in way or another made the completion of the thesis even smoother.

Special thanks to Mohammed Elmusrati, Hasan Elsallabi, and Abdulla Abouda for the fruitful discussions and scientific debates we have had. I wish to express my warm gratitude to all Libyan Ph.D., M.Sc. and graduated students in Finland for providing a home away from home.

Finally, I am deeply indebted to my mother, brothers and sisters in Libya and to my wife for her care, patience and support.

This work is dedicated to the memory of my father Gumaa Farag Tarhuni

Contents

Abstract ii

Preface iii

List of Publications vii

List of Figures x

Abbreviations xi

Symbols xii

1 Introduction 1

1.1 Motivation . . . 1
1.2 Main Research Contributions . . . 2
1.3 Thesis outline . . . 3

2 CDMA Techniques in Optical Communications 5

2.1 Background . . . 5
2.1.1 Wavelength Division Multiplexing . . . 5
2.1.2 Time Division Multiple Access . . . 6
2.2 Code Division Multiple Access . . . 7
2.2.1 Optical Frequency-Hopping CDMA . . . 8
2.2.2 Spectral Phase and Intensity Encoding . . . 9
2.2.3 Temporal OCDMA . . . 10
2.2.4 Optical Orthogonal Codes . . . 11
2.2.5 Prime Codes (PC) . . . 16
2.3 State of Polarization Encoding [P6] . . . 18
2.3.1 Stoke and Jones spaces . . . 19
2.3.2 Polarization Shift Keying . . . 21
2.3.3 SOP-CDMA system . . . 22

3 Multi-class and Polarized-Optical Orthogonal Codes **27**
3.1 Multi-Class Optical Orthogonal Codes [P1] 27
3.1.1 Multiclass-OOC code generation 28
3.1.2 Multiclass-OOC Interference Model 31
3.1.3 Multiclass-OOC BER performance 33
3.2 Polarized-OOC [P2] 35
3.2.1 Multiclass Polarized-OOC 36

4 Optical Power Control **39**
4.1 Optical Power Control: Optical Pre-amplified Star Network [P3] 40
4.1.1 Centralized Optical Power Control: Noise-Free 41
4.1.2 Centralized Optical Power Control: ASE noise non-negligible 42
4.1.3 Centralized Optical Power Control: Network Partitioning 43
4.1.4 Distributed Optical Power Control 44
4.2 Optical Power Control for Multirate Data Traffic [P4] 45
4.2.1 Spectral Radius Analysis 46
4.2.2 Rate reduction algorithm 48
4.3 Optical Nonlinear Power Control (ONPC) [P5] 50
4.3.1 Convergence Analysis of the ONPC Algorithm 51
4.3.2 ONPC Feasibility 53

5 Conclusions **55**
5.1 Thesis results 55
5.2 Future Work 56

Bibliography **58**

Publications **64**

List of Publications

This work is based on the following appended publications. Throughout the thesis, the publications are referred to by the following labels [P1] to [P6]. In all included publications, the author of this thesis was the main contributor in terms of ideas, theory, simulations, and writing. Mohammed Elmusrati has helped with the convergence analysis part of [P3] and [P5]. He was also participating in theoretical discussions about the contents of [P1], [P4] and [P6].

[P1] **Naser Tarhuni**, Timo Korhonen, Edward Mutafungwa, and M. Elmusrati, "Multi-Class Optical Orthogonal Codes for Multi-Service Optical CDMA Networks", *Journal of Lightwave Technology*, Vol.24, Issue 2, Feb. 2006, Pages: 694-704.

[P2] **Naser Tarhuni**, M. Elmusrati, and T. Korhonen, "Polarized Optical Orthogonal Codes for Optical Code Division Multiple Access Systems", *Progress in Electromagnetics Research PIER*, 65, Pages: 125-136, 2006.

[P3] **Naser G. Tarhuni**, Timo O. Korhonen, Mohammed Elmusrati, and Edward Mutafungwa, "Power Control of Optical-CDMA Star Networks," *Optics Communications journal*, Vol. 259, Issue 2, March 2006, Pages: 655-664.

[P4] **Naser Tarhuni**, M. Elmusrati, and T. Korhonen, "Multi-Class Optical-CDMA Network Using Optical Power Control," *Progress in Electromagnetics Research PIER*, 64, Pages: 279-292, 2006.

[P5] **Naser Tarhuni**, M. Elmusrati, and T. Korhonen, "Nonlinear Power Control for Asynchronous Fiber-optic CDMA Networks," *IEEE International Conference on Comm. ICC 2006*, Volume 6, Pages:2782 - 2786, June 2006.

[P6] **Naser Tarhuni**, Timo O. Korhonen, and Mohammed Elmusrati, "State of Polarization Encoding for Optical Code Division Multiple Access Networks," *Journal of Electro-Magnetic Waves and Applications JEMWA* scheduled for publication, Volume 21, Number 10, Pages:1313-1321, 2007.

List of Figures

2.1 Time-Frequency multiple access space diagrams. 6
2.2 Schematic of star coupled optical CDMA network. 7
2.3 Fiber Bragg grating encoder and decoder. 9
2.4 (a) Spectral Phase optical CDMA system, (b) Schematic illustration of optical Fourier transform and spectral phase encoding. 10
2.5 Parallel delay lines encoder for OOC. 11
2.6 Input (left) and output (right) optical pulses for [1,4,5] OOC code. 11
2.7 Two (13,3,1) OOC's and their autocorrelation and cross-correlation. 13
2.8 An optical correlator receiver.. 14
2.9 Bit error rate for OOC, number of users K = 20. 15
2.10 Autocorrelation and cross-correlation of a prime sequence with $q = 5$. . . . 17
2.11 Bit error probability for prime codes. 18
2.12 The Poincaré sphere. 20
2.13 Polarization modulator. 21
2.14 Optical PolSK BER for the antipodal and orthogonal 2-PolSK. 22
2.15 Optical antipodal 2-PolSK BER for a complete axis rotation over maximum circle for SNR of 12,14 and 15 dB. 23
2.16 Optical SOP-CDMA, (a) transmitter, (b) receiver. 24
2.17 Eye Diagram for 3-user SOP-CDMA using (a) Gold (b) Hadamard; codes after 20 km SMF. 25

3.1 Flowchart of the Multiclass OOC code construction algorithm. 29
3.2 Bit error rate for a two-class OOC system as a function of the code weight of the low rate class. 34
3.3 Bit error rate for a two-class OOC system as a function of the code length of the second class. 34
3.4 Mark positions and differences for a (N,3) polarized-OOC. 35

4.1 An optical CDMA star network with K users. 40
4.2 Number of supported nodes satisfying the target SIR in a Prime coded network with and without power control. Prime number of 31. 45
4.3 Estimated and theoretical PDF of $\rho(\mathbf{\Lambda H})$. 47
4.4 Rate-Reduction algorithm. 48

4.5 CDF of spectral radius with different RRs. 49
4.6 Target and actual SIR variations of the far and close nodes. 54

Abbreviations

ASE	Amplified Spontaneous Emission
BER	Bit Error Rate
DWDM	Dense Wavelength Division Multipling
E/O	Electrical-to-Optical conversion
EDFA	Erbium Doped Fiber Amplifier
FBG	Fiber Bragg Grating
FH-OCDMA	Frequency Hopping Optical Code Division Multiple Access
FWM	Four Wave Mixing
IM-DD	Intensity Modulation Direct Detection
LCM	Liquid Crystal Modulator
MAI	Multiple Access Interference
MPD	Mark Position Difference
MWML-OOC	Multi-Weight Multi-Length Optical Orthogonal Code
MWSL-OOC	Multi-Weight Single-Length Optical Orthogonal Code
O/E	Optical-to-Electrical conversion
OCDMA	Optical Code Division Multiple Access
ONPC	Optical Nonlinear Power Control
OOC	Optical Orthogonal Code
OOK	ON-OFF Keying
OTDMA	Optical Time Division Multiple Access
PC	Prime Code
PolSK	Polarization Shift Keying
SIR	Signal to Interference Ratio
SMF	Single Mode Fiber
SOP	State of Polarization
SPM	Self Phase Modulation
SWML-OOC	Single-Weight Multi-Length Optical Orthogonal Code
WADM	Wavelength Add Drop Multiplexer
WDMA	Wavelength Division Multiple Access

Symbols

D_i	Set of MPDs associated with i-th code
d_n	n-th element of the set of MPDs
$E_{x(y)}$	Electric field in the x (y)-direction
G_{amp}	Optical amplifier gain
I_q	Total MAI affecting q-th class codes
K	Number of users in OCDMA
N_q	OOC code length of class q
N_{sp}	ASE noise power
P_E or $P(E)$	Bit error probability
$P_{\max}$	maximum transmit optical power
Q	Number of classes in multiclass OOC
q	Prime number
$R_{C_iC_j}$	Correlation between two signature signals C_i and C_j
U_i	Position of i-th Mark in the OOC code
W_q	OOC code weight of class q
Δ_q	Set of remaining differences after generating all i-th classes with $1 \leq i \leq q$
γ_i	SIR of the i-th node
Γ_{max}	maximum achievable carrier to interference power ratio
Γ_{min}	minimum target carrier to interference power ratio
λ_a	OOC Autocorrelation constraint
λ_c	OOC Crosscorrelation constraint
$\|\mathbf{C}\|$	Number of elements in set $\mathbf{C}$
$\mathbf{C}$	OOC code set
$\mathbf{D}_{OOC}$	Total set of possible MPDs for the OOC
$\mathbf{J}$	Jones vector representation of the optical field
$\mathbf{P}$	Power vector
$\mathbf{S}$	Stoke vector representation of the optical field
μ	Threshold
$\phi_{x(y)}$	Phase of the electric field in the x (y)-direction
$\Re$	Photodiode responsitivity
$\rho(\mathbf{H})$	Spectral radius of matrix $\mathbf{H}$
σ	Average variance of crosscorrelation amplitude between codes
θ	Azimuth angle of the optical field
ε	Elipticity of the optical field
G_{ij}	Total optical power attenuation between transmitting node j and receiving node i
H_{ij}	Interference matrix elements

Chapter 1

Introduction

1.1 Motivation

The past decade has witnessed significant development in the area of optical networking. Such advanced technologies as Dense Wavelength Division Multiplexing (DWDM), optical amplification, optical path routing (wavelength cross-connect), wavelength add-drop multiplexer (WADM), and high-speed switching have found their way into the wide-area networks (WANs), resulting in a substantial increase of the telecommunications backbone capacity and greatly improved reliability [1]. At the same time, enterprise networks almost universally converged on 100 Mbps Fast Ethernet architecture. Some mission-critical local area networks (LANs) even moved to 1000 Mbps rates, courtesy of a new Gigabit Ethernet standard recently adopted by the IEEE. On the user access side, the most widely deployed "broadband" solutions today are digital subscriber line (DSL) and cable modem (CM) networks. Although they are improvements compared to 56 kbps dial-up lines, they are unable to provide enough bandwidth for emerging services such as video-on-demand (VoD), interactive gaming, or two-way video conferencing [2]-[4]. Therefore, we need to search for a new and versatile approach that enables a cost effective with more than enough bandwidth to accommodate end-user data-rate intensive applications. One approach that can do the job is CDMA which is proven effective in the wireless regime. The optical version of CDMA, called Optical CDMA (OCDMA), is expected to inherit many of the advantages of the wireless version with the added value of fiber optic huge bandwidth. Because of its unique features, OCDMA is gaining increased attention in the research community which is indicated by the increased number of publications in different conference and journal papers.

Several challenging points of research are still missing for practical OCDMA realization and development. These include, the high Multiple Access Interference (MAI) naturally present in almost all forms of OCDMA, increasing network capacity in terms of number of concurrent users, and codes that can support various traffic demands in terms of bandwidth and Bit Error Rate (BER) performance. Furthermore, it is logical to search for new OCDMA implementations that can meet the expected performance requirements in a sim-

ple and cost effective way.

The objectives of this thesis, based on the aforementioned challenges, are threefold. First, the development of new code designs that can support multiclass traffic demands. These codes are derived from existing ones so that they are easy to implement and evaluate. The second objective is to adopt and apply well known power control concepts from the wireless schemes and propose new algorithms suitable for optical domain in order to alleviate the performance floor set by the MAI. Finally, we propose a new OCDMA approach by exploiting the polarization properties of the optical field.

The expected improvement in channel utilization and relatively low technical complexity and ease of implementation will have a direct impact on current optical networking trends. By providing simple, very high speed, and cost effective optical access network systems based on the proposed techniques, this will be beneficial for example in at-home health care monitoring systems and other applications requiring high-rate high-QoS networks. In addition, by allowing more optically-encoded CDMA signals at the same time we avoid the costly process of deploying new fiber lines.

1.2 Main Research Contributions

The primary contributions of the research work presented in this thesis are in the general area of OCDMA networking. The contributions of this thesis are summarized in the following.

1. Optical Orthogonal Codes (OOCs) are well known for incoherent optical CDMA networks:

   (a) Using an algorithmic approach we proposed and constructed multiclass OOCs in [P1]. Focus is placed on the flexibility and simplicity of the construction technique. The target was to extend existing OOCs to support variable traffic data rates. Several examples of the constructed codes are tabulated in [P1]. The next step is to analyze an OCDMA network based on the developed multiclass OOC. The major obstacle is to evaluate the probability density function of the MAI. We proposed the use of Poisson approximation to model the MAI which significantly simplifies BER calculations with acceptable accuracy.

   (b) In [P2], we modified the OOC by the use of polarization axis and developed the *Polarized-OOC*. Our aim is to enhance the capacity of OCDMA networks in terms of number of concurrent users. We showed that the number of users in the polarized-OOC is two times the conventional OOC. Also, a method of fiber-induced polarization rotation is proposed in [P2]. Polarized-OOC based OCDMA system is investigated using advanced optical simulators that solves the nonlinear schrodinger equation.

2. Publications [P3], [P4], and [P5] concentrate on applying power control to OCMDA:

(a) In [P3] the basic power control is applied to demonstrate the validity of the concept and the expected gain in such system. Network partitioning is proposed also to simplify optimum power calculations. Emphasis is put on optical amplifier noise as the main noise source. Also upper bound on the achievable Signal-to-Interference-Ratio (SIR) is evaluated. Application of distributed algorithms is investigated and convergence analysis is conducted.

(b) The use of power control for multiclass traffic is analyzed in [P4]. We focused on the spectral radius of the network matrix as the main system parameter rather then the BER since the spectral radius identifies feasible solutions of the optimum power control problem. We also proposed a rate reduction algorithm to increase network feasibility to more than 98%.

(c) In [P3] and [P4] we use the optical SIR and therefore the effect of photodetection nonlinearity was not considered. In [P5] we proposed and analyzed the nonlinear power control algorithm by taking into account the photodetection nonlinearity. Convergence analysis of the proposed algorithm is also given.

3. In [P6] we proposed a new OCDMA system based on the state-of-polarization encoding. Only preliminary work has been done on this topic.

1.3 Thesis outline

The thesis is composed of a summary part and a collection of publications. In the summary part we summarize the results and material included in the appended publications as follows. Background material and basic OCDMA techniques are reviewed in Chapter 2. Also, in Chapter 2 we present the proposed polarization-encoding OCDMA system. In Chapter 3 we discuss the extension of OOCs to support multiclass traffic. also, the polarization axis is used to increase the number of supported users. In Chapter 4, power control is applied including centralized, distributed and nonlinear power control. Finally, conclusions and future work are given in Chapter 5.

Chapter 2

CDMA Techniques in Optical Communications

In order to make full use of the available bandwidth in optical fibers and to satisfy the bandwidth demand in future information networks, it is necessary to multiplex low rate data streams onto optical fiber to increase the total throughput. This chapter is a review of basic OCDMA systems classified as, Temporal, Spectral phase and amplitude, and Frequency Hoping OCDMA. Also, the use of Polarization-encoding for OCDMA is introduced at the end of the chapter.

2.1 Background

The three major multiple access schemes are shown in Fig. 2.1.

2.1.1 Wavelength Division Multiplexing

In a Wavelength Division Multiple Access (WDMA) system, each channel occupies a narrow (> 100GHz) optical bandwidth around a center wavelength or frequency [5, 6]. The modulation format and speed at each wavelength can be independent of those of other channels. Arrayed or tunable lasers will be needed for WDMA applications [7, 8]. Because each channel is transmitted at a different wavelength, they can be selected using an optical filter [9]. Tunable filters can be realized using acousto-optics [10], liquid crystal [11], or fiber Bragg grating [12]. To increase the capacity of the fiber link using WDMA we need to use more carriers or wavelengths, and this requires optical amplifiers [13] and filters to operate over extended wavelength ranges. Due to greater number of channels and larger optical power the increased nonlinear effects in fibers causes optical crosstalk such as four-wave mixing [14] over wide spectral ranges. Another approach to increase the capacity of WDMA links is to use Dense WDM (DWDM) [15], which will have to operate with reduced channel spacing (ITU-T recommendation G.692 defines 43 wavelength channels from 1530-1565 nm, with a spacing of 100 GHz). This requires a sharp optical filter with linear phase response, wavelength stable components, optical amplifiers with flat

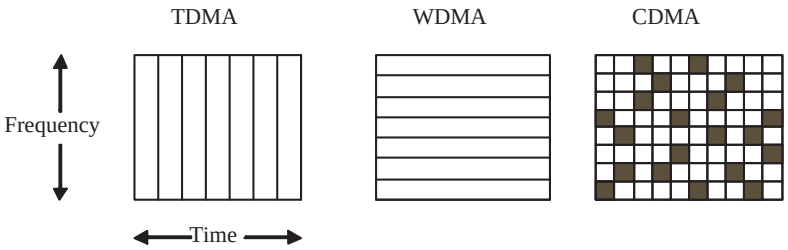

Figure 2.1: Time-Frequency multiple access space diagrams.

gain over wide bandwidths, and optical fibers must support hundreds of channels without distortion or crosstalk. With respect to channel switching, wavelength routing is the next switching dimension for DWDM, with interferometric crosstalk being an essential issue in the implementation of cross-connects based on space and wavelength [16]. Hence, the extent of wavelength routing that is realizable places fundamental limits on network flexibility, which in turn determines switch size and flexibility.

2.1.2 Time Division Multiple Access

Digital communications allow the possibility of Time Division Multiple Access (TDMA). In a TDMA system, each channel occupies a pre-assigned time slot, which interleaves with the time slots of other channels. SDH (Synchronous Digital Hierarchy) is the current transmission and multiplexing standard for high-speed signals, which is based on time division multiplexing [17]. Optical TDMA (OTDMA) networks can be based on a broadcast topology or incorporate optical switching [18]. In broadcast networks, there is no routing or switching within the network. Switching occurs only at the periphery of the network by means of tunable transmitters and receivers. The switch-based networks perform switching functions optically within the network in order to provide packet-switched services at very high bit rates [19]. In an electrically time-multiplexed system, multiplexing is carried out in the electrical domain, before the electrical-to-optical conversion (E/O). Demultiplexing is carried out after optical-to-electrical conversion (O/E). Major electronic bottlenecks occur in the multiplexer E/O, and the demultiplexer O/E, where electronics must operate at the full multiplexed bit rate (number of channels $\times$ bit rate of individual channels). Alternatively, in optically time-multiplexed systems where by moving the E/O and O/E converters to the baseband channels the electronic bottlenecks are alleviated [20]. OTDMA systems offer a large number of node addresses; however, the performance of OTDMA systems is ultimately limited by the time-serial nature of the technology. OTDMA systems also require strong centralized control to allocate time slots and to maintain synchronous operation.

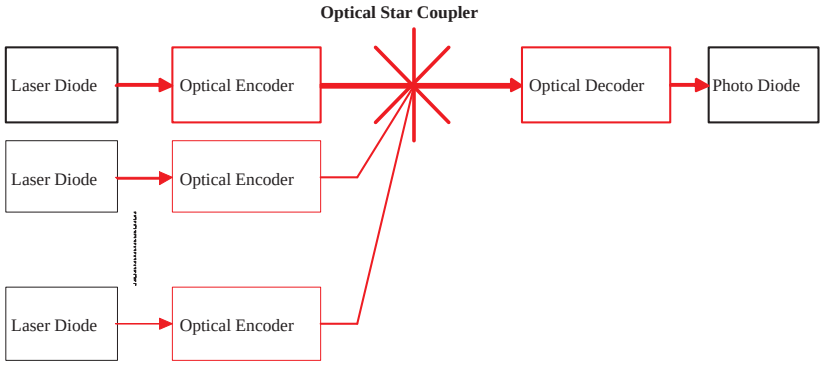

Figure 2.2: Schematic of star coupled optical CDMA network.

2.2 Code Division Multiple Access

The concept of code multiplexing spans the electromagnetic communication spectrum, but differing device capabilities and constraints unique to each spectral domain influence the details of implementation [21]. The roots of CDMA are found in Spread Spectrum communication techniques [22, 23]. OCDMA offers an interesting alternative for LANs because neither time management nor frequency management of all nodes is necessary. OCDMA can operate asynchronously, without centralized control, and does not suffer from packet collisions (in case of well designed codes with reduced multi-user interference); therefore, very low latencies can be achieved. Dedicated time or wavelength slots do not have to be allocated, so statistical multiplexing gains can be high. In contrast to OTDMA and WDMA where the maximum transmission capacity is determined by the total number of these slots (i.e., hard-limited), OCDMA allows flexible network design because the BER depends on the number of active users (i.e., soft-limited) [24].

A variety of approaches to OCDMA have been suggested [25]- [27]. They share a common strategy of distinguishing data channels not by wavelength or time slot, but by distinctive spectral or temporal code (or signature) impressed onto the bits of each channel. Suitably designed receivers isolate channels by code-specific detection. A typical OCDMA system is shown in Fig. 2.2, where the nodes are connected through a passive $N \times N$ star coupler. At the logical level this configuration is a broadcast-and-select network. Other network topologies can be used for OCDMA such as bus and ring topologies. There is no global optimum topology for fiber optic LAN interconnection. Each topology has its own advantages and disadvantages, which may become significant or insignificant depending on the specific application under consideration [28].

In intensity ON-OFF-Keying (OOK) system, each user information source modulates the laser diode directly, (or indirectly using an external modulator). The optical signal is encoded optically in an optical encoder that maps each bit into a very high rate (code length

$\times$ data rate) optical sequence. The encoded optical signals from all active users are broadcasted in the network by a star coupler. The star coupler can be a passive or active device. The optical decoder or matched filter at the receiving node is matched to the transmitting node giving a high correlation peak that is detected by the photodetector. Other users using the same network at the same time but with different codes give rise to MAI. This MAI can be high enough to make the LAN useless if the code used in the network does not satisfy specific cross-correlation properties. Other factors affecting the performance of the network are shot noise and thermal noise at the receiver.

Generally, OCDMA systems can be classified to Incoherent or Coherent schemes. Incoherent schemes are based on Intensity Modulation-Direct Detection (IM-DD) scheme that incorporates non-coherent, direct detection of superimposed optical power of all users. The operation of direct detection makes the procedure simple and the receiver is cost effective. Because of the way optical signals are detected in IM-DD systems using the photodiode, optical systems are considered as positive or unipolar systems [29, 30]. The photo detector detects the power of the optical signal but not the instantaneous phase variations of the optical signal. Thus, only incoherent signal processing techniques can be used to process the signature sequences composed of only ones and zeros restricting the type of codes that can be used in incoherent OCDMA systems [31]. In coherent OCDMA, the phase information of the optical carrier is crucial for the despreading process. Due to the nature of optical fiber transmission and its phase noise limitations, such as nonlinear effects of Self Phase Modulation (SPM), Four Wave Mixing (FWM) and random phase fluctuations, the complexity of the coherent OCDMA receiver makes this approach more difficult to realize.

Alternatively, OCDMA can be classified into Temporal OCDMA and Spectral OCDMA according to the way the optical signal is encoded. Temporal OCDMA performs the coding in time domain by using very short optical pulses (e. g., 10 ps at data rate 1 Gbps and code length of 100) using optical delay lines to compose the coded optical signal. Spectral OCDMA, on the other hand, codes the phase or intensity of the spectral content of a broadband optical signal by using phase or amplitude masks. Optical Frequency hopping can be considered as a temporal-spectral coding where the coding is done in both dimensions.

2.2.1 Optical Frequency-Hopping CDMA

Fast optical frequency-hop code division multiple access (FH-CDMA) system based on fiber Bragg grating can be used for high rate LANs [32, 33]. Multiple Bragg gratings are used to generate the CDMA hopping frequencies. Due to the linear "first in, first reflected" nature of multiple Bragg gratings, the time frequency hopping pattern is determined by the order of the grating frequencies in the fiber. The order of the grating frequencies in the decoder is the reverse of that in the encoder to achieve the matched filtering operation. Fig. 2.3 shows the encoder and decoder in a star coupled network. If the central wavelength of the incoming optical wave is equal to the Bragg wavelength, it will be reflected by the fiber Bragg grating, or it will be transmitted. With proper written CDMA coding pattern, the

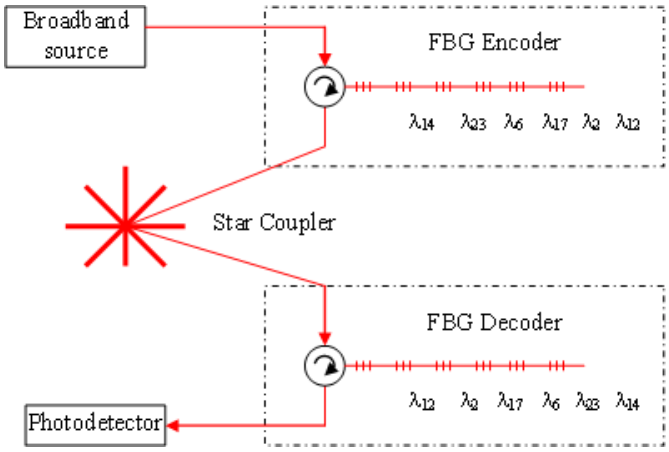

Figure 2.3: Fiber Bragg grating encoder and decoder.

reflected light field from fiber Bragg gratings will be spectrally encoded onto an address code. To reduce the effect of the MAI, codes with minimum cross-correlation properties are required. Bin [34] proposed a novel FH-code generation algorithm. These codes fall into the category of one-coincidence sequences and are characterized by the following three properties:

1. All of the sequences are of the same length;
2. In each sequence, each frequency is used at most once;
3. The maximum number of hits between any pair of sequences for any time shift equals one.

2.2.2 Spectral Phase and Intensity Encoding

Coherent spectral phase encoding was first proposed by [26] and [35]. Fig. 2.4(a) shows an encoder and decoder of the spectral phase encoding system. The information source modulates the very short optical pulse of the laser. The generated short pulses are Fourier transformed and the spectral components are multiplied by the code corresponding to a phase shift of 0 or π. Fourier transform can be implemented by the Grating and lens pair as shown in Fig. 2.4(b).

As a result of phase encoding, the original sharp ultra-short optical pulse is transformed into a low intensity signal with longer duration. The Liquid Crystal Modulator (LCM) is used in [36] to set the spectral phase to maximum-sequence phase. The LCM has a fully programmable linear array and individual pixels can be controlled by applying drive levels resulting in phase shifts of 0 or π. By a phase mask, the dispersed bandwidth of a pulse is partitioned into N_c frequency chips, where each chip has the width $\Omega = W/N_c$. Each chip is assigned a phase shift depending on the user's PN code. Another approach for spectral

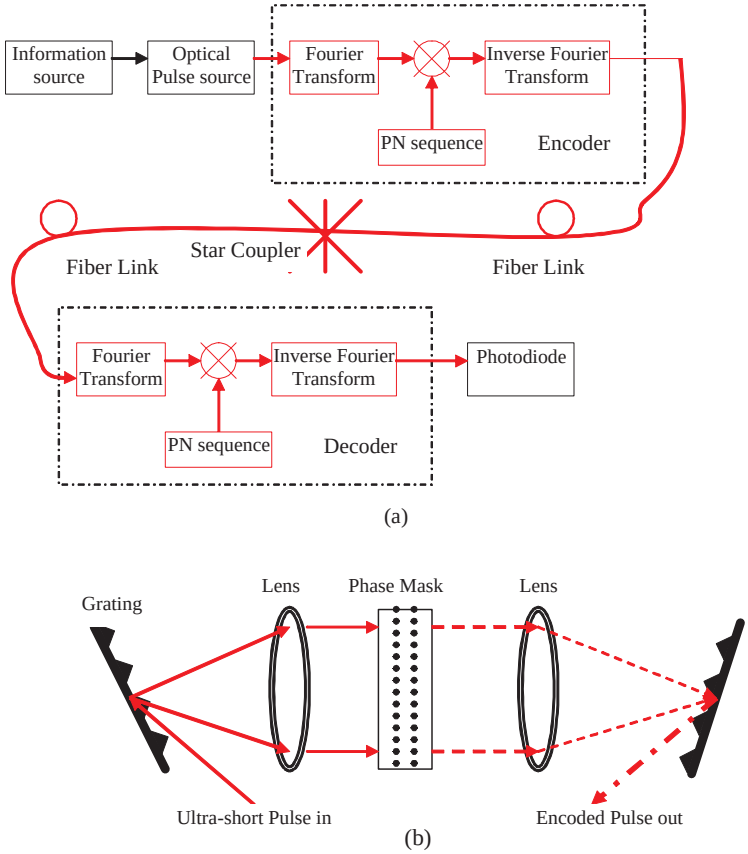

Figure 2.4: (a) Spectral Phase optical CDMA system, (b) Schematic illustration of optical Fourier transform and spectral phase encoding.

optical CDMA encoding called non-coherent spectral intensity encoding is used in [37]-[40]. This approach is similar to the coherent spectral phase encoding but instead of the phase mask an amplitude mask is used to block or transmit certain frequency components. At the receiver, balanced photodetectors are used to detect the signal. The received optical signal is split into two beams, the first beam is filtered with the same amplitude mask used at the transmitter, and the second beam is filtered by the complement of the mask. The two filtered optical beams are detected by a balanced receiver, thus by subtraction it is possible to achieve full orthogonality.

2.2.3 Temporal OCDMA

The Temporal OCDMA signal can be generated by the splitting and combining of very short optical pulses in a parallel optical delay line encoder. A high-peak optical pulse is encoded into a low intensity pulse train using a parallel optical delay line network at the transmitter (Figures 2.5, 2.6). The decoding is performed by intensity correlation at the receiver using a matched network of optical delay lines. Because of the positive nature of

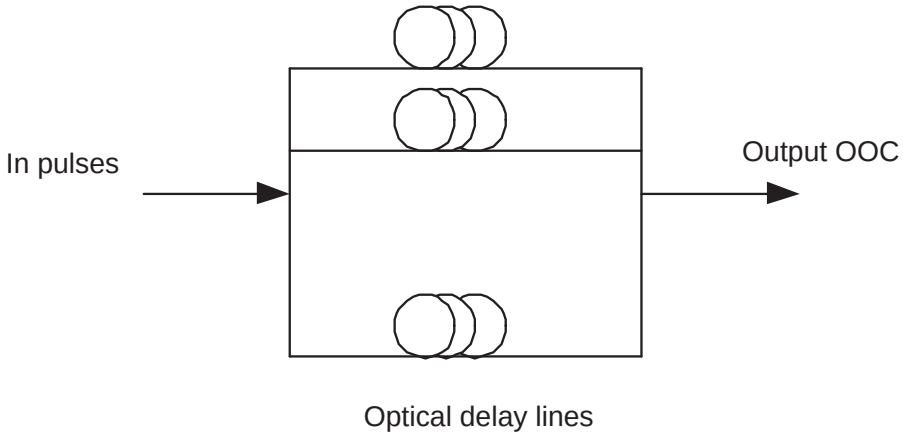

Figure 2.5: Parallel delay lines encoder for OOC.

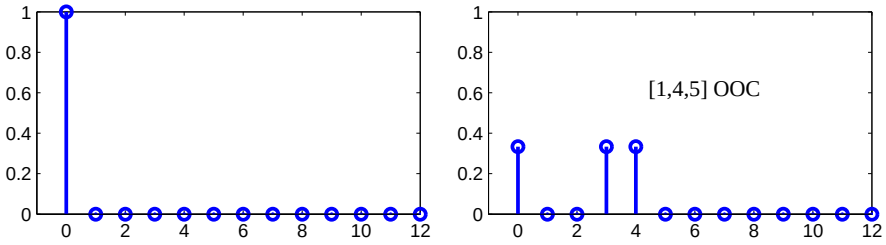

Figure 2.6: Input (left) and output (right) optical pulses for [1,4,5] OOC code.

the detection scheme, the interference is quit high.

Although capable of generating any code sequence, the configuration in Fig. 2.5 is very hardware limited. Also, high power loss can be a limiting factor of this type of encoders [41]. Tunable implementation of the encoding and decoding operations of the optical delay line can be used to allow flexible addressing [42].

2.2.4 Optical Orthogonal Codes

An important type of temporal codes is the OOC proposed for IM-DD OCDMA systems [43]-[49]. OOCs can be generated using the scheme shown in Fig. 2.5 [50]-[56]. These are very sparse codes, meaning that the code weight is very low, thus limiting the efficiency in practical coding and decoding. Moreover, the number of codes that can be supported is very low as compared to a code set with the same length used in RF communications (PN codes for example). To get more codes we need to increase the length of the code, demanding the use of very short pulse optical sources having pulse width much smaller than the bit duration.

OOC Properties

The required temporal OCDMA codes must satisfy the following conditions:

a) The peak autocorrelation function of the code should be maximized.

b) The side lobes of the autocorrelation function of the code should be minimized.

c) The cross-correlation between any two codes should be minimized.

Conditions a) and c) insure that the MAI is minimized, while condition b) simplifies the synchronization process at the receiver. If synchronous optical CDMA is used, then condition b) makes it possible to use one code for all users, which may reduce the coding and decoding complexity.

The correlation $R_{C_iC_j}(\tau)$ of two signature signals $C_i(t)$ and $C_j(t)$ is defined as,

$$R_{C_iC_j}(\tau) = \int_{-\infty}^{\infty} C_i(t)C_j(t+\tau)dt, \quad \text{for } i,j = 1,2,..., \tag{2.1}$$

Where the signature signal $C_k(t)$ is defined as,

$$C_k(t) = \sum_{n=-\infty}^{\infty} c_k(n)p_{T_c}(t-nT_c), \quad \text{for } k = 1,2,... \tag{2.2}$$

$c_k(n) \in \{0,1\}$ is a periodic sequence of period N. The discrete correlation function $R_{c_ic_j}(m)$ between any two sequences $c_i(n)$ and $c_j(n)$ is given by,

$$R_{c_ic_j}(m) = \sum_{n=0}^{N-1} c_i(n)c_j(n+m), \quad \forall m = ...,-1,0,1,2... \tag{2.3}$$

The sum in the argument of $c_j(n+m)$ is calculated modulo N, we represent this operation from now on as $[x]_y$ which reads x modulo y. In the discrete form, the above conditions are rewritten as:

a) The number of ones in the zero-shift discrete autocorrelation function should be maximized.

b) The number of coincidences of the non-zero shift discrete autocorrelation function should be minimized.

c) The number of coincidences of the discrete cross-correlation function should be minimized.

An OOC is usually represented by a quadruple, $(N, W, \lambda_a, \lambda_c)$, where N is the sequence length, W is the sequence weight (number of ones), λ_a is the upper bound on the autocorrelation for non-zero shift and λ_c is the upper bound on cross-correlation. The conditions for optical orthogonal codes are,

$$R_{c_ic_i}(m) = \sum_{n=0}^{N-1} c_i(n)c_i(n+m) \leqslant \lambda_a, \quad [m]_N \neq 0 \tag{2.4}$$

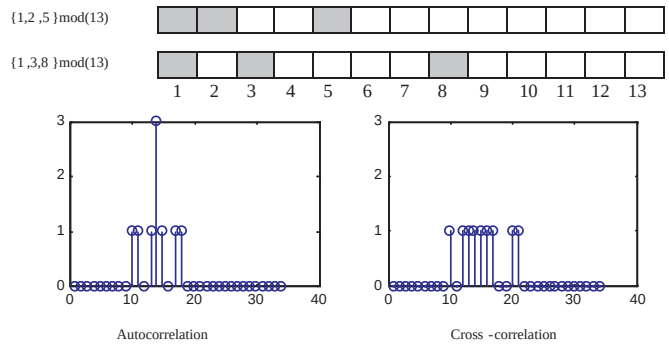

Figure 2.7: Two (13,3,1) OOC's and their autocorrelation and cross-correlation.

$$R_{c_i c_j}(m) = \sum_{n=0}^{N-1} c_i(n)c_i(n+m) \leqslant \lambda_c, \quad \forall m \tag{2.5}$$

When $\lambda_a = \lambda_c = 1$, the OOC is represented by (N, W) and called strict OOC. It can be shown that the number of codes is upper-bounded by [43],

$$K \leqslant \left\lfloor \frac{N-1}{W(W-1)} \right\rfloor \tag{2.6}$$

where $\lfloor x \rfloor$ denotes the integer portion of the real number x. An example of a strict OOC (13,3) code set is $\mathbf{C} = \{1100100000000, 1010000100000\}$, plotted in Fig. 2.7. It is clear from the figure that the peak autocorrelation is equal to the code weight of 3, and the non-zero shift autocorrelation and the cross-correlation is less than or equal to one. The same code set $\mathbf{C}$ can be represented using the set notation as $\mathbf{C} = \{[1, 2, 5], [1, 3, 8]\} mod(13)$, where the elements in the set represent the position of the pulses in the code.

Mark Position Differences

Generally, we can represent the OOC as a set of pulse (Mark) positions. Using the set notation we represent each code by,

$$C_k = [U_1, U_2, ..., U_W], \quad U_1 = 1 \tag{2.7}$$

where U_n is an integer number indicating the position of the n-th Mark. Using the set notation, conditions (2.4) and (2.5) can be rewritten as,

$$|(C_i + m) \cap (C_i + n)| \leqslant \lambda_a \tag{2.8}$$

for any $C_i \in \mathbf{C}$ and any integers $[m]_N \neq [n]_N$ and,

$$|(C_i + m) \cap (C_j + n)| \leqslant \lambda_c \tag{2.9}$$

for any $C_i, C_j \in \mathbf{C}$ and any integers m and n. Now define a set of Mark Position Differences (MPDs) for the code as,

$$D_i = \{d_1, d_2, ..., d_{W(W-1)}\} \tag{2.10}$$

where d_n is the difference between Mark positions in (2.7) and given by,

$$d_n = \quad N - [N + U_i - U_j]_N \,, \quad i \neq j; i, j = 1, 2, ..., W \tag{2.11}$$

For a code of length N, the MPD is limited to a set of integer numbers,

$$\mathbf{D}_{OOC} = \{1, 2, 3, ..., N-1\} \tag{2.12}$$

The correlation properties (2.8) and (2.9) for a strict OOC means that the code mark difference set D_i must be unique and contains no duplications. If a difference set D_i contains repeated elements, then the auto-correlation property is violated and the auto-correlation is larger than 1. If $D_i \cap D_j \neq \Phi$ then the cross-correlation property is violated and the cross-correlation is larger than 1. Then from (2.12) and (2.10) the upper bound on the number of codes in the strict OOC is obtained as in (2.6).

OOC BER performance

Assume that the performance degradation is due to only the MAI, meaning that the effects of other noise sources are neglected. Also the light sources are assumed to be incoherent sources, which lead to addition of active users' optical intensity. Assume that all users have equal average power. The k^{th} baseband signal at the output of the k^{th} optical encoder can be represented as [43],

$$s_k(t) = B_k(t) C_k(t) \tag{2.13}$$

where $B_k(t) = \sum_{n=-\infty}^{\infty} b_k(n) p_T(t - nT)$ is the binary data signal with $b_k(n)$ is the binary data sequence of the k^{th} user and T is the bit period with $T/T_c = N$. The transmitters are not time synchronous, thus, the received signal at the front end of each receiver's decoder is given by,

$$r(t) = \sum_{k=1}^{K} s_k(t - \tau_k) \tag{2.14}$$

where τ_k is the time delay associated with the k^{th} signal. Without loss of generality, the delay for the desired user is assumed to be zero and the other interfering users have a

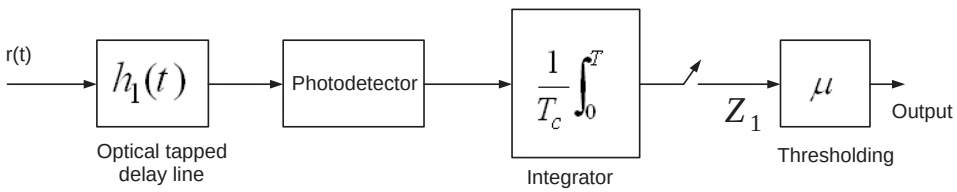

Figure 2.8: An optical correlator receiver..

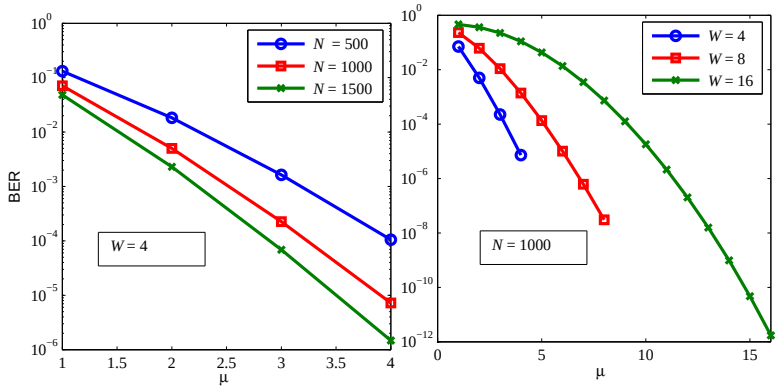

Figure 2.9: Bit error rate for OOC, number of users K = 20.

delay of less than one bit period which is a multiple of the chip period (chip synchronous case). This chip synchronous scenario gives the upper bound on the bit error probability. The receiver is a correlation operation with an impulse response equal to the time reversal of the encoder. Several receiver structures for OCDMA are evaluated in [31, 57]. A typical optical receiver of OCDMA with passive optical correlator is shown in Fig. 2.8.

In this ideal case the MAI will be binomially distributed with parameters p and K, where $p = W^2/2N$ is the hit probability (probability of success) and K the number of active users (Number of trials). Therefore, the probability of error for the chip-synchronous and noise-free OCDMA system is calculated from [44],

$$P(E) = \sum_{i=\mu}^{K-1} \begin{pmatrix} K-1 \\ i \end{pmatrix} \left(\frac{W^2}{2N}\right)^i \left(1 - \frac{W^2}{2N}\right)^{K-1-i} \tag{2.15}$$

where μ is the threshold. The BER for OOC for different code structures is shown in Fig. 2.9, where the effect of the code length and the effect of code weight are clear from the plots. Since the above analysis ignores the noise, therefore setting $W - 1 < \mu \leq W$ results in the minimum BER. If the threshold is set to $\mu > W$, then the output is always zero for any input data and the BER reaches the worst case of 0.5. Longer codes enhance the performance of the system but with the requirement of very short chip duration. Codes with larger weights perform better but with the restriction of less number of supported users and higher optical power loss due to hardware implementation.

Optical hard-limiters can be used to enhance the performance of the OOC system. Even though they are not realizable for optical domain, single and double hard-limiters are proposed in [29, 31, 44] and [58]. The hard-limiters are inserted to remove undesired optical signal fluctuations before and after the decoding operation.

In deriving the performance of OOC system in (2.15) the only contamination taken into account is the MAI. In real optical receivers several noise mechanisms affect the performance.

Assuming an OCMDA system with OOC coding and an APD detector, the compound effect of APD noise, thermal noise and MAI was evaluated in [59]. The complex statistics of the APD is described in [60] was not used but instead a simplifying Gaussian approximation [61] was applied in [59]. It was shown that when the noise effects are considered, the performance of OCDMA based on OOCs can be two orders of magnitude worse than that of the ideal case. Also the improvement in BER by using hard-limiters is not significant because the MAI during the zero data bit transmission cannot be completely suppressed as in the noise-free case.

Although synchronization of OCDMA systems is beyond the scope of the thesis it is important to point out briefly to some of the work done on the topic. In the above, asynchronous operation was assumed but synchronization of optical OOC systems will be a major requirement to introduce burst and packet-based systems. Also performance degradation of OOC systems will be sever if synchronization is not maintained. A simple synchronization method was considered in [62] and more recently a multiple search method that reduce the mean synchronization time was proposed and analyzed in [63].

The main disadvantage of OOCs is the limited number of users for a reasonable code length and weight, therefore, two dimensional OOC codes that use the wavelength-time dimensions were proposed and their performance analysis and construction methods were thoroughly investigated [64]- [66].

2.2.5 Prime Codes (PC)

OOCs presented in last section lacks the availability of a systematic way of code construction that can be used at both ends of the communication links. Codes have to be constructed beforehand (using iterative random search, combinatorial techniques, etc.) and some sort of lookup table is needed for each user. On the other hand, the OOC is a highly sparse code and the number of supported users can be very low, hence, another important type of codes proposed for OCDMA is the prime code [50]-[67]. The prime code has a higher correlation value as compared to the OOC but it can support more users. Furthermore, the ease of generation of prime codes makes them a good candidate for OCDMA networks.

The prime code consists of many blocks each containing a single pulse. For any prime number q, a code comprises q blocks of length q. A set of code sequences of length $N = q^2$, derived from prime sequences of length q, where q is a prime number, was derived in [50]. The procedure for code generation starts with the Galois Field, $GF(q) = \{0, 1, ..., j, ..., q-1\}$, then a prime sequence $S_k = \left(s_{k0}, s_{k1}, ..., s_{kj}, ..., s_{k(q-1)}\right)$ is evaluated by multiplying each element j of the *GF(q)* by an element k of *GF(q)* modulo q. q distinct prime sequences can thus be obtained which is mapped into a time-mapped binary code

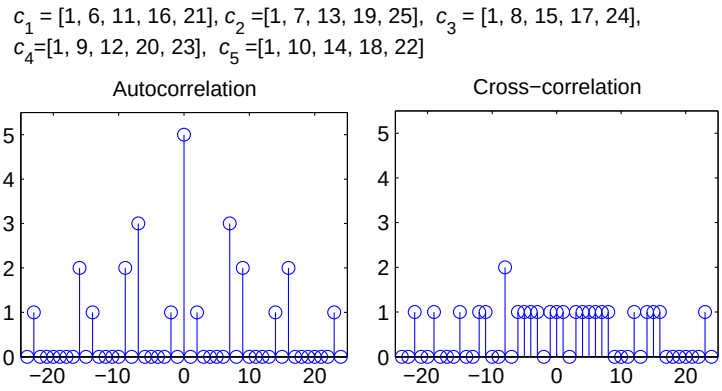

Figure 2.10: Autocorrelation and cross-correlation of a prime sequence with $q = 5$.

$c_k = (c_k(0), c_k(1), ..., c_k(j), ..., c_k(N-1))$ according to,

$$c_k(n) = \begin{cases} 1 & \text{for } n = s_{kj} + jq; s_{kj} = k \odot j; \\ 0 & otherwise \end{cases} \tag{2.16}$$

where $j = 0, 1, ..., q-1$ and $\odot$ means modulo q multiplication. Fig. 2.10 shows the $q = 5$ prime code in mark position set format along with the autocorrelation of c_3 and cross-correlation between c_3 and c_4. It is known that the peak autocorrelation of prime sequences is q, non-zero shift maximum autocorrelation of $q-1$, and maximum cross-correlation of 2, thus prime sequences can be considered as an OOC with
$\left(N = q^2, W = q, \lambda_a = q-1, \lambda_c = 2\right)$. The high non-zero shift autocorrelation of prime codes make the synchronization much more difficult at the receiving end. On the other hand, more users can be addressed using prime codes than with OOC of the same length and weight. Additionally, the prime codes can be generated more efficiently using a parallel-serial network of delay lines and switches [42]. When K users are transmitting simultaneously, the total interference at a given receiver is the superposition of K – 1 different cross-correlation functions. The average variance of the cross-correlation amplitude, computed using all possible code sequences for several values q of the prime code was found to be approximately [56],

$$\sigma^2 \approx 0.29 \tag{2.17}$$

and the SIR is given by

$$SIR = \frac{q^2}{\sigma^2 (K-1)} \tag{2.18}$$

Using the Gaussian approximation for large number of users, the probability of error can be approximated as,

$$P_E = Q\left(\frac{\sqrt{SIR}}{2}\right) \approx Q\left(\frac{q}{\sqrt{1.16\,(K-1)}}\right) \tag{2.19}$$

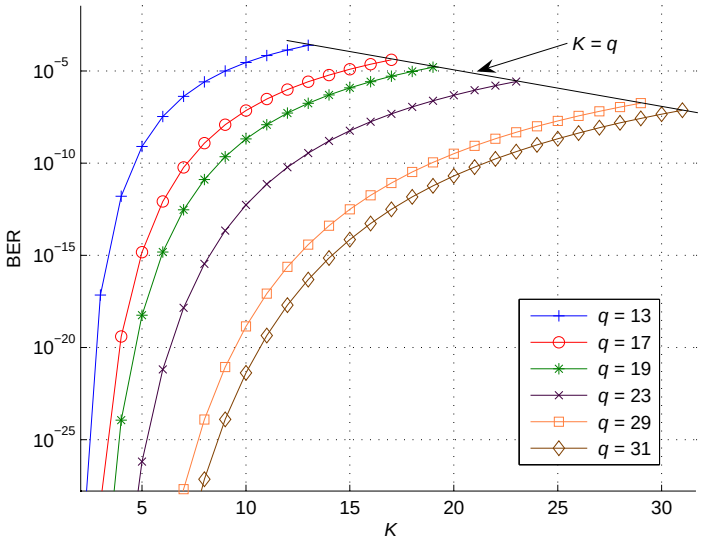

Figure 2.11: Bit error probability for prime codes.

Prime code BER plot is shown in Fig. 2.11 for $q = 17$ to $q = 31$. To reduce the maximum cross-correlation value of a prime code from 2 to 1, each sub-block in the prime code words is padded with q-1 or more trailing zeros. This is the Extended Prime Code (EPC) sequence that can be constructed using the following procedure,

$$c_k(n) = \begin{cases} 1 & \text{for } n = s_{kj} + j\,(2q-1)\,; s_{kj} = k \odot j; j = 0, 1, ..., q-1 \\ 0 & \text{otherwise} \end{cases} \tag{2.20}$$

The extended prime sequence has the same code cardinality and weight, but the code length is now increased to $q(2q-1)$, thus the extended prime code can be considered as an OOC with $(N = q(2q-1), W = q, \lambda_a = q-1, \lambda_c = 1)$. The error probability of the extended prime code is reduced such that the factor multiplying the number of interferers in (2.19) is reduced from 1.16 to 0.75 [67].

2.3 State of Polarization Encoding [P6]

Polarization Shift Keying (PolSK) was considered during recent years as a digital modulation candidate for the optical fiber communications [68]-[71]. The applicability of PolSK is a result of the property that an orthogonal state of polarization (SOP) pair from a monochromatic light source at the input of the single mode fiber (SMF) leads to orthogonal SOP pair at the fiber output, although the input SOP is not maintained in general. Previous experimental work showed that the depolarization phenomena along the fiber and polarization dependent losses are negligible even after relatively long fiber spans [72]-[74].

A polarization control device is required at the receiving end of the fiber to counteract the polarization transformations occurring along the optical fiber. Polarization spreading was proposed in [75] in order to make the performance of PolSK independent of such transformations without the need for costly polarization control. The spreading waveforms used were simply staircase, linear, and sinusoidal waveforms. A similar approach which is called polarization scrambling was used in [76]-[78] to overcome the problem of polarization hole burning in Erbium-Doped Fiber Amplifiers (EDFA) used in transoceanic lightwave systems. Measurements on buried SMF fibers reported in [79] reveal that polarization fluctuations are quite slow and can vary typically between 2^o-10^o per day. Therefore, a quasi-static scenario can be assumed, in which several blocks of coded data bits suffer from constant polarization offset which can be easily compensated.

In addition to the many advantages of optical CDMA, the use of SOP-encoding is expected to inherit several Polarization Shift Keying (PolSK) advantages such as higher immunity to laser phase noise [80], resistance to self-phase modulation and cross-phase modulation attributed to fiber Kerr nonlinearities [81].

2.3.1 Stoke and Jones spaces

An optical signal propagating along the z-axis will have the transversal electric field components given by,

$$\left.\begin{array}{l} E_x = a_x\left(t\right)e^{j\phi_x(t)} \\ E_y = a_y\left(t\right)e^{j\phi_y(t)} \end{array}\right\} \tag{2.21}$$

where a_x, a_y, ϕ_x and ϕ_y are the amplitude and phase of the x and y-components, respectively. Then the electrical field vector is given by,

$$\vec{E} = (E_x\vec{x} + E_y\vec{y})e^{j\omega_0 t} \tag{2.22}$$

where ω_0 is the optical frequency. Using the Jones representation [82], the field can be represented by the vector,

$$\mathbf{J} = [E_x, E_y]^T \tag{2.23}$$

assuming that the intensity of the beam has been normalized so that $|E_x|^2 + |E_y|^2 = 1$. Two polarization states represented by $\mathbf{J}_1$ and $\mathbf{J}_2$ are orthogonal if the inner product is zero, i.e., $\mathbf{J}_1^H\mathbf{J}_2 = E_{1x}^*E_{2x} + E_{1y}^*E_{2y} = 0$, where H is the Hermitian operation. The Jones vectors, $[1,0]^T$, $[0,1]^T$, $[\cos(\theta), \sin(\theta)]^T$, $\frac{1}{\sqrt{2}}[1,j]^T$, and $\frac{1}{\sqrt{2}}[1,\text{-}j]^T$ represent the linearly horizontal in x-direction (LPX), linearly vertical in y-direction (LPY), linearly with angle θ inclined on x-direction (LPθ), right circularly polarized (RCP), and left circularly polarized (LCP) waves respectively.

The SOP of a fully polarized lightwave can be described also by the Stokes parameters [82],

$$\left.\begin{array}{c} S_1 = a_x^2 - a_y^2 \\ S_2 = 2a_xa_y\cos\left(\phi\right) \\ S_3 = 2a_xa_y\sin\left(\phi\right) \end{array}\right\} \tag{2.24}$$

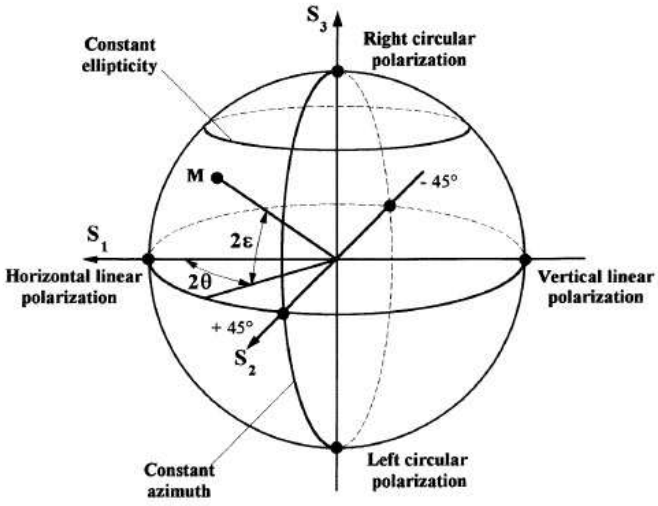

Figure 2.12: The Poincaré sphere.

with $\phi = \phi_y - \phi_x$. Then the total power density of the optical beam can be evaluated from the Stokes parameters as follows,

$$S_0^2 = S_1^2 + S_2^2 + S_3^2 \tag{2.25}$$

In Stokes space, a vector with a constant power density spanning a sphere of radius S_0 is called "Poincaré sphere" (Fig. 2.12). For a beam intensity normalized to one, the Stoke parameters are equivalently divided by S_0 and the normalized Stoke vector is given by $\mathbf{S} = [S_1, S_2, S_3]^T/S_0$. We have the following facts:

- Orthogonal SOPs map into antipodal points on the Poincaré sphere, i.e., when $\mathbf{J}_1^H \mathbf{J}_2 = 0$ then $\mathbf{S}_2 = -\mathbf{S}_1$.
- All linear polarizations lie on the plane $[S_1, S_2]^T$.
- The points $\pm S_0 \vec{s}_3$ represent the two circular SOP's.
- The other points represent elliptic SOP's.

The ellipticity ε and the azimuth θ are determined from the S_i elements by the following two relations:

$$\varepsilon = \frac{1}{2} \tan^{-1} \left(\frac{S_3}{(S_1^2 + S_2^2)^{1/2}} \right) \tag{2.26}$$

$$\theta = \frac{1}{2} \tan^{-1} \left(\frac{S_2}{S_1} \right) \tag{2.27}$$

Any SOP can be transformed into another by multiplying it with a Mueller matrix. Mueller matrices for ideal polarizers, rotators and retarders required for SOP processing can be

found in [83]. The rotator operator is a unitary matrix that multiplies input SOP to result in the output SOP. In order to counteract the SOP fiber induced rotation we proposed a simple technique in [P2]. Assuming that a reference SOP $\mathbf{S}_t$ is launched at the fiber input and the received SOP at the fiber output is measured and denoted by $\mathbf{S}_r$. A matrix $\mathbf{R}$ that can rotate $\mathbf{S}_r$ around $\mathbf{S}_{av} = [S_{av1}, S_{av2}, S_{av2}]^T = (\mathbf{S}_t + \mathbf{S}_r)/2$ by an angle π is used to fully compensate the fiber-induced SOP rotation.

2.3.2 Polarization Shift Keying

In PolSK, the angle of one polarization component is switched relative to the other between two angles, therefore, binary data bits are mapped to two Jones (Stoke) vectors. One possible realization of polarization switching is the modulator shown in Fig. 2.13. When the switching angle is 180^o or 90^o, then we get antipodal constellation $\mathbf{S}_{(0)} = [0, 1, 0]^T$, $\mathbf{S}_{(1)} = [0, -1, 0]^T$, or orthogonal constellation $\mathbf{S}_{(0)} = [0, 1, 0]^T$, $\mathbf{S}_{(1)} = [0, 0, 1]^T$, respectively. Where we normalized the Stokes points by S_0. The first case represents antipodal constellation points (orthogonal SOPs) on the Poincaré sphere.The second case corresponds to what we call orthogonal constellation which means that the points are at an angle of 90^o to each other. Note that orthogonal constellation and orthogonal SOP are two different concepts. The antipodal constellation above can be generated using (2.21) and (2.22) by substituting $\phi_y(t) - \phi(t)_x = \pi d(t)$, while the orthogonal constellation is generated by $\phi_y(t) - \phi(t)_x = \frac{\pi}{2} d(t)$ where $d(t)$ is the binary data. When noise is added to the optical beam, the constellation points will move randomly over the sphere.

At the receiver, the optical beam is split into two orthogonal polarizations that should be aligned to the reference axis of the incoming field. Each beam is detected separately and the received Stoke parameters are evaluated. The dot product (correlation) is performed between the received Stoke vector and the two possible transmitted Stoke vectors. The decision is made in favor of the maximum. This can be described visually as the operation of dividing the sphere into two hemispheres by a plane orthogonal to the line joining the two constellation points (antipodal constellation case) at the sphere center. Then the estimated Stoke point corresponds to that constellation point in the same hemisphere. In Fig. 2.14 the probability of bit error (BER) is numerically evaluated and plotted for antipodal and

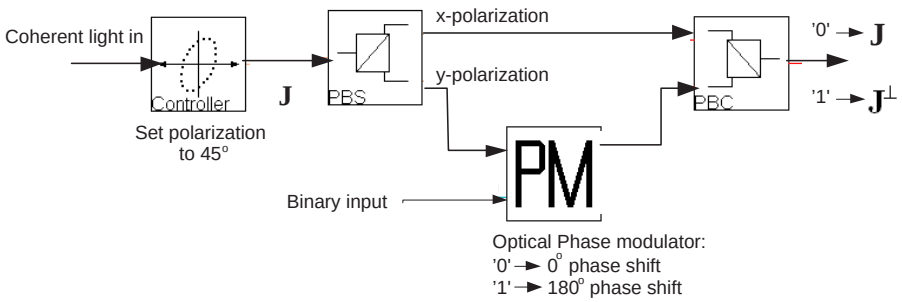

Figure 2.13: Polarization modulator.

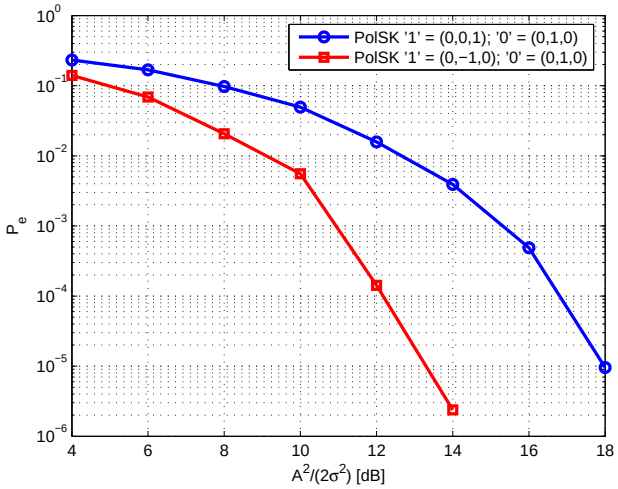

Figure 2.14: Optical PolSK BER for the antipodal and orthogonal 2-PolSK.

orthogonal constellation points where it is assumed that the noise variance on the x- and y-polarizations is the same and denoted by σ^2. As expected the antipodal constellation results in lower BER performance due to the largely spaced points on the sphere. Remember that the points can move only on the surface of the sphere. The results are in agreement with the theoretical analysis presented in [80] in which the exact BER performance for the antipodal constellation was evaluated to be,

$$P(E) = \frac{1}{2}\exp(-\gamma/2) \tag{2.28}$$

where $\gamma = A^2/(2\sigma^2)$ is the SNR and A is the magnitude of the electric field component.

To evaluate the effect of constellation rotation on 2-PolSK, we simulate a scenario of full rotation over a maximum circle on the same plane of the constellation points. The SNR is set to 12, 14 and 15 dB and the result is shown in Fig. 2.15. The curve reveals the fact that the BER deteriorates if the reference system used at the receiver is different from that of the incoming signal. When the relative angle of rotation is close to 90^0 and 270^0 the error approaches the worst case of 0.5 due to the fact that at these angles the constellation points are at the boundary of the decision used at the receiver. Thus a small drift in the received constellations due to noise will move the points across the boundary plane leading to bit errors.

2.3.3 SOP-CDMA system

In Fig. 2.16 a schematic diagram of the proposed optical SOP-CDMA system is shown. The light source is a highly coherent laser with a fully polarized SOP. If an unpolarized source is used, then a polarizer can be inserted after the laser source. The polarized beam passes through the SOP encoding (PolM) which switches the SOP of the input beam between

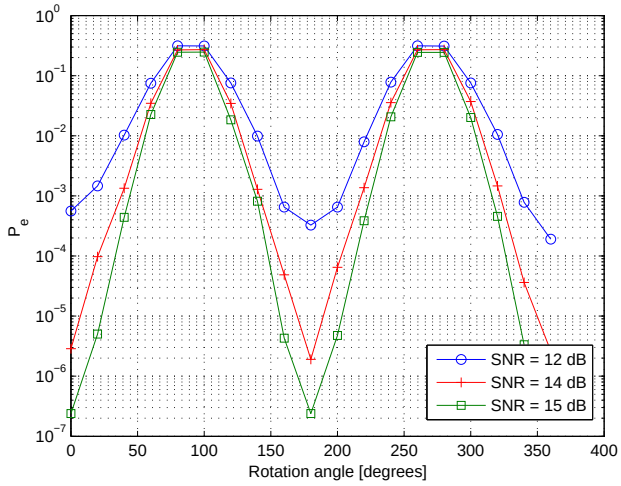

Figure 2.15: Optical antipodal 2-PolSK BER for a complete axis rotation over maximum circle for SNR of 12,14 and 15 dB.

two orthogonal states N times per bit according to an externally supplied code (such as Hadamard, or Gold codes). For a K-user system with the first user as the desired one, the k-th user SOP encoded signal can be written as,

$$\mathbf{J}_k(t) = \begin{cases} \mathbf{J}_{(0)} & \text{if } d_k(t) \oplus c_k(t) = 0 \\ \mathbf{J}_{(1)} & \text{if } d_k(t) \oplus c_k(t) = 1 \end{cases} \tag{2.29}$$

for $k = 1, 2, ..., K$, where $d_k(t) = \sum_{i=-\infty}^{\infty} d_{k,i} P_T(t - iT)$ and $c_k(t) = \sum_{i=-\infty}^{\infty} c_{k,i} P_{T_c}(t - iT_c)$ are the data and code signals with $d_{k,i}, c_{k,i} \in \{0, 1\}$ and $P_T(t)$ is a unity rectangular pulse starting at zero and of width T, and $\oplus$ is the XOR operation. For simplicity we assume that the emitted light is initially linearly polarized at an angle of 45^o, therefore, $\mathbf{J}_{(\mathbf{0})} = \frac{1}{\sqrt{2}}[1, 1]^T$ and $\mathbf{J}_{(\mathbf{1})} = \frac{1}{\sqrt{2}}[-1, 1]^T$. At the receiver end we have the desired signal Jones vector corrupted by multiaccess interference and additive Gaussian noise as,

$$\mathbf{J}_r(t) = \begin{bmatrix} E_{rx} \\ E_{ry} \end{bmatrix} = \mathbf{J}_1(t) + \sum_{k=2}^{K} \mathbf{J}_k(t) + \mathbf{J}_n(t) \tag{2.30}$$

where $\mathbf{J}_n = [E_{nx}, E_{ny}]^T$ is the complex Jones vector of the additive white noise.

The received composite signal is passed through a splitter (assumed lossless). For the upper (lower) branch the composite signal is alternately switched according to a code (code complement) which is assumed synchronized to the applied one at the transmitter side. Then the polarization transformer rotates the input polarization by 45^o in order to align the output beam polarization to the polarizer axis which is selected here for simplicity and without loss of generality to be the x-polarization axis. The polarizer will pass only the optical beam matched to its axis. The upper branch and lower branch signals are denoted by the superscript $(\cdot)^{(0)}$ and $(\cdot)^{(1)}$ respectively. Details of evaluating the decision variable

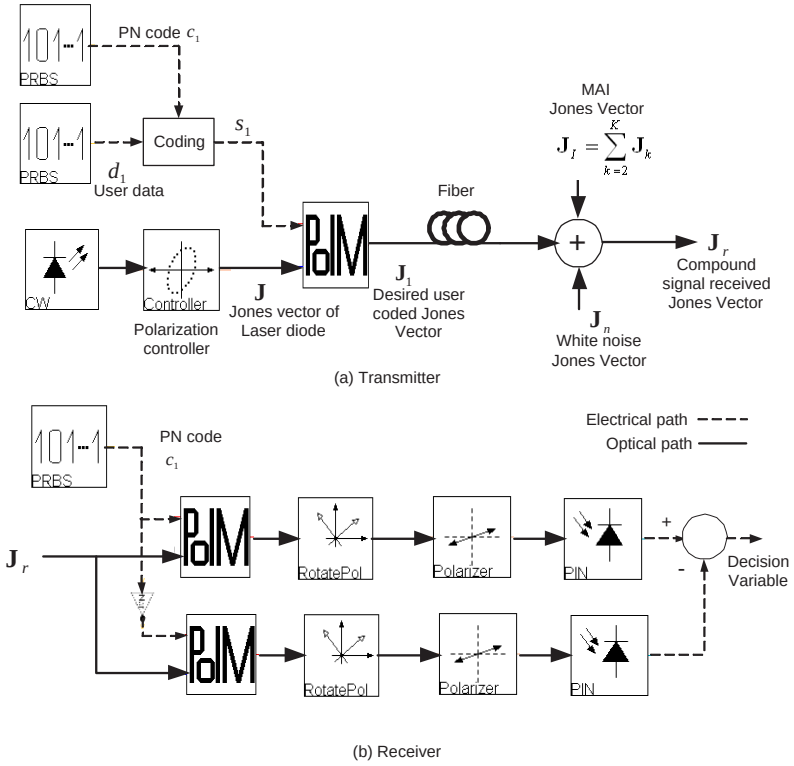

Figure 2.16: Optical SOP-CDMA, (a) transmitter, (b) receiver.

are given in [P6]. After expanding and some algebra we get,

$$D^{(i)} = \frac{|E_{rx}|^2 + |E_{ry}|^2}{2} + |E_{rx}|\,|E_{ry}| \cos\left(\Phi + x_i \pi\right) \tag{2.31}$$

where $\Phi = \text{ang}\,(E_{ry}) - \text{ang}\,(E_{rx})$. The decision variable is the difference between the upper and lower branch outputs which is formulated as follows,

$$D = \int_0^T (D^{(1)} - D^{(0)}) dt \tag{2.32}$$

And the decision is made according to the following rule,

$$\hat{d}_1 = \begin{cases} 0 & \text{if } D < 0 \\ 1 & \text{if } D \geq 0 \end{cases} \tag{2.33}$$

The performance of the SOP-CDMA system is inspected numerically by applying two kind of codes, namely, Gold and Hadamard codes. For a data rate of 100 Mb/s, a simulation reported in [P6] showed the eye diagram (reproduced in Fig. 2.17 for convenience) and the Q-factor. It is shown that the Hadamard based SOP-CDMA system is superior to the Gold

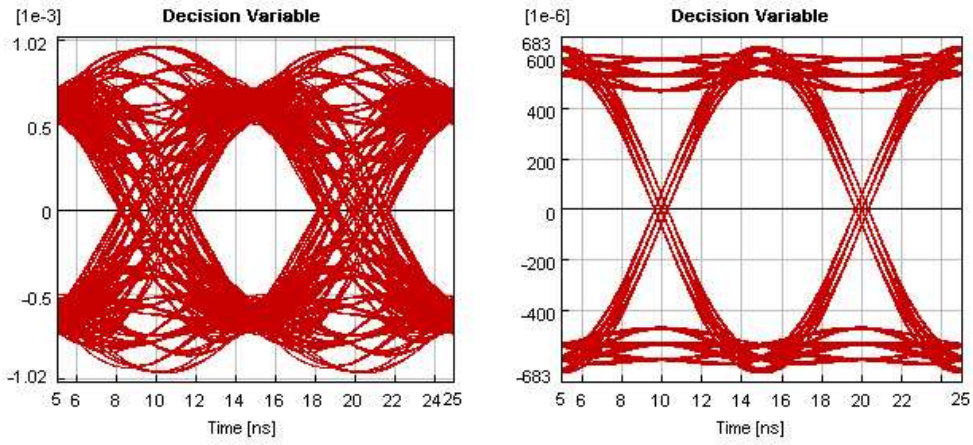

(a) Gold (b) Hadamard

Figure 2.17: Eye Diagram for 3-user SOP-CDMA using (a) Gold (b) Hadamard; codes after 20 km SMF.

code based system. The main disadvantage of the Hadamard code is that it is designed for synchronous implementation. This will not be a difficult task to achieve in fixed topology networks as the considered optical star network.

Chapter 3

Multi-class and Polarized-Optical Orthogonal Codes

Optical CDMA based networks are an interesting alternative to support various traffic types of multimedia applications with highly variable performance targets. Generally, multi-length codes are designed to support multi-rate services, while the multi-weight codes are designed to support differentiated quality of service (QoS) for multimedia applications. However, existing OOCs are limited to single class or multiclass with restricted weight and length properties. Therefore, there exits a lack of flexibility in the existing OOCs to support arbitrary rate and QoS.

This chapter investigates the generation of suitable codes to support multirate traffic. Concentrating on the OOCs, a generation method based on the concept of MPDs and random search approach is presented. Performance analysis is also conducted for the multiclass OOC. Next the Polarized-OOC is introduced, which is proposed as an extension to the OOCs and multiclass OOCs in order to allow more concurrent users to the network.

3.1 Multi-Class Optical Orthogonal Codes [P1]

Several multirate optical CDMA transmission schemes has been thoroughly investigated in the literature. In [84], a multirate optical CDMA transmission was achieved by varying the length of the code set whose auto- and cross-correlation is constrained to be three or smaller. This limits the system applications due to the relatively high error probability for high rate users. A parallel mapping scheme was applied to multirate optical CDMA in [85]. The scheme is based on assigning a number of code sequences according to the user data rate. This limits the applicability because of the limited number of available codes. The authors in [86] proposed a double-weight two-dimensional OOC based on Galois field theory, unfortunately the proposed OOCs are able to support only two different services without multi-rate compatibility. Recently, variable weight OOCs constructions based on two schemes called balanced pairwise design and packing design with partition are given [87]. In the second scheme variable-weight OOCs are constructed by partitioning

larger weight codeword into a family of codes with a smaller code weight. On the other hand, multi-length OOC was presented in [88] with fixed code weights. The rates of the constructed code set cannot be selected arbitrarily because short codewords are used to construct longer ones. Moreover, the performance analysis was presented for a double-rate case only. In [89] the variable rate OOC for video applications with fixed weight was proposed. The performance analysis in terms of the bit error rate of the system is not considered. A flexible implementation of the tapped delay line for applications to variable length OOC can be found in [90].

In [91], we discussed a two-class OOC and the performance of such system was evaluated based on the assumption that the binomially distributed OOC interference is approximated by a Gaussian distribution. This approximation is valid only if the number of users is high and the probability of collision from an interfering user is close to 0.5. This assumption fails to be accurate in OOCs with long code lengths and low code weights.

In order to support variable data rates and QoSs in optical CDMA network based on OOCs, it is highly desirable to have variable length and variable weight codes. The shorter the codes are, the higher the rates are, and the higher the code weights are the higher the QoSs. These two code parameters have earlier been investigated in literature separately under code length and weight restrictions. In this regard we generate an OOC set with arbitrary code length and/or code weight while preserving the required correlation properties of the strict OOC. This allows then the different codes to be assigned for different user classes. The code set construction is also flexible in such a way that the code length and weight can be selected arbitrarily as long as the number of desired codes in each class of users can be supported. We can categorize the multiclass code into:

- Multi-Weight, Single-Length OOC (MWSL-OOC): This is beneficial in systems with fixed data rates supporting different QoS, since the signal to interference ratio in optical networks employing OOC and perfect matched filtering is proportional to the square of the code weight.
- Single-Weight Multi-Length OOC (SWML-OOC): This is applicable to systems with equal QoS and supporting variable data rate.
- Multi-Weight Multi-Length OOC (MWML-OOC): In this case the weights and lengths of the multiclass OOC are selected arbitrarily.

3.1.1 Multiclass-OOC code generation

Assume that we have a Q-class system where each class is represented by the length, weight pairs (N_q, W_q) with $N_1 \leq ... \leq N_q ... \leq N_Q$ and the number of users in the q-th class is K_q. The code set can be represented by $\mathbf{C} = \{C_1, C_2, ..., C_q, ..., C_Q\}$ where $C_q = \{c_{1,q}, c_{2,q}, ..., c_{K_q,q}\}$ is the set of codes in class q and each $c_{m,q}$ is the set of mark position representation (see (2.7)) of the m-th code in the q-th class. The total number of

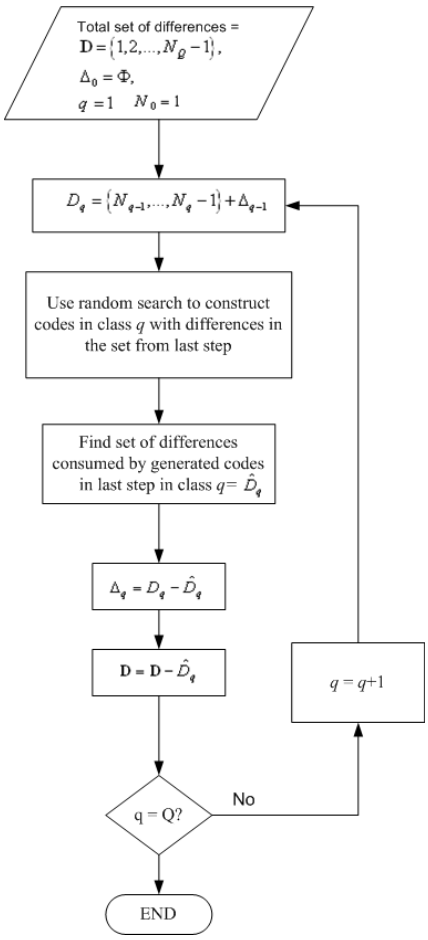

Figure 3.1: Flowchart of the Multiclass OOC code construction algorithm.

codes in the multiclass OOC code set is $K=\sum_{q=1}^{Q}K_q$ and the total set of allowed differences in class q is $D_q=\{1,2,...,N_q-1\}$. Associated with each code $c_{m,q}$ is a set of MPDs $d_{m,q}$ according to (2.10) with a length of $W_q(W_q-1)$. Then the differences consumed by K_q codes in class q is denoted by $\hat{D}_q$ with the number of elements equal to $K_qW_q(W_q-1)$. In addition to that, the allowed difference set of the multiclass code is limited by the length of the longest code as $\mathbf{D}=\{1,2,...,N_Q-1\}$. Let Δ_q denotes the set of remaining differences after generating all i-th classes with $1\leq i\leq q$. Then the MPD construction technique of the multiclass code set $\mathbf{C}$ is outlined as shown in Figure 3.1.

It should be emphasized that the proposed multiclass OOC code generation presented here makes use of the existing techniques in finding $c_{m,q}$, that is a computationally demanding task for higher code weights when random search is applied. However, in the investigated media access scheme the required codes are sparse, and their code weights are low. On the other hand, since the optical power loss in the currently available encoding technology (based mainly on power splitting and combining) grows as $10\log(W)$ dB. Therefore,

lower weight codes are only of practical importance. Furthermore, since the code set is assumed to be available before any real system implementation, hence, the speed of the code generation algorithm is of minor importance.

It should be also noted that repeated application of the algorithm results in multiple code sets with the same weight and length parameters. The availability of multiple multiclass OOC code sets with the same (N_q, W_q) can be used to enhance the security of the system. This can be implemented by instructing the users to switch to other multiclass OOCs with the same parameters from time to time. For more information on OCDMA security refer to [92]. For example, Table 3.1 lists three alternatives to the three-class OOC tabulated in [P1, Table III] and characterized by High Rate High QoS (550,7), Medium Rate Medium QoS (930,5), and Low Rate Low QoS (1300,3). Only part of the generated codes are shown and each time the algorithm is restarted we get a new set of codes.

The prove of existence of an optimal OOC $(N, W, 1)$ code set for general values of N and W is prohibitive and mathematically complex problem. However, it has been considered for specific values of the code weight and length. For example, the authors in [93] considered the special case of an OOC with $(N, 4, 1)$ and concluded that in order to obtain an optimal OOC the code length should be restricted to 6(mod 12) and 24(mod 48). Therefore, investigation of the cardinality optimality of the MWML-OOC is not further discussed in this thesis. Alternatively, we consider only the upper bound on each class cardinality conditioned on the number of codes in the other classes. For a $Q-$class MWML-OOC with a given (N_q, W_q), the upper bound on the q-th class cardinality is a function of (N_q, W_q), K_i, and W_i for $i < q$. This is summarized in the following,

A Q-class, strict MWML-OOC code set $\mathbf{C}$ *is represented by the length and weight pairs* (N_q, W_q) *where* $N_1 \leq N_2 \leq ... \leq N_q ... \leq N_Q$. *The cardinality* $|\mathbf{C}|$, *and the number of codes in the q-th class* K_q *is given by,*

$$|\mathbf{C}| = K = \sum_{q=1}^{Q} K_q \tag{3.1}$$

subject to the constraint of,

$$\frac{\sum_{q=1}^{Q} K_q W_q (W_q - 1)}{N_Q - 1} \leqslant 1 \tag{3.2}$$

and,

$$K_q \leqslant \left\lfloor \frac{N_q - N_{q-1} + |\Delta_{q-1}|}{W_q(W_q - 1)} \right\rfloor \tag{3.3}$$

As an example, consider the two OOCs with (500, 7) and (1000,7) then the number of supported users in each class separately is less than or equal to 11 and 23 respectively. If we use the same parameters to jointly design a multiclass OOC then the number of users for the shortest length code is first set to some given value less than 11, say 5, then the upper bound for the second class is evaluated as 18.

Table 3.1: Three-realizations of three-class strict MWML-OOC code set.

Realization 1.

(550,7)	(930,5)	(1300,3)
[1, 26, 78, 127, 188, 206, 535]	[1, 294, 540, 621, 920]	[1, 187, 384]
[1, 113, 219, 277, 351, 398, 449]	[1, 210, 233, 317, 848]	[1, 583, 696]
[1, 96, 211, 256, 265, 403, 417]	[1, 227, 475, 614, 660]	[1, 7, 578]
[1, 31, 32, 136, 314, 340, 406]	[1, 259, 522, 582, 672]	[1, 270, 411]
	[1, 262, 552, 576, 692]	[1, 1012, 1265]
	[1, 706, 733, 743, 776]	[1, 40, 967]
	[1, 87, 155, 405, 761]	[1, 100, 755]
	[1, 118, 363, 367, 580]	[1, 57, 424]
	[1, 167, 468, 658, 740]	[1, 164, 507]
		[1, 422, 807]

Realization 2.

(550,7)	(930,5)	(1300,3)
[1, 19, 87, 260, 482, 499, 545]	[1, 15, 347, 555, 884]	[1, 268, 727]
[1, 171, 212, 238, 289, 404, 498]	[1, 123, 366, 888, 926]	[1, 114, 778]
[1, 16, 214, 295, 402, 507, 526]	[1, 85, 127, 227, 463]	[1, 92, 1289]
[1, 91, 187, 285, 421, 487, 520]	[1, 184, 369, 454, 508]	[1, 177, 181]
	[1, 180, 596, 736, 756]	[1, 751, 894]
	[1, 419, 644, 764, 772]	[1, 583, 1110]
	[1, 115, 283, 608, 882]	[1, 373, 489]
	[1, 219, 229, 721, 786]	[1, 343, 902]
	[1, 228, 881, 903, 904]	[1, 801, 1266]
		[1, 231, 307]

Realization 3.

(550,7)	(930,5)	(1300,3)
[1, 146, 154, 272, 378, 379, 499]	[1, 84, 124, 641, 773]	[1, 316, 1193]
[1, 22, 380, 397, 479, 537, 548]	[1, 179, 754, 815, 835]	[1, 488, 1142]
[1, 17, 65, 67, 211, 314, 358]	[1, 189, 455, 565, 727]	[1, 232, 1226]
[1, 27, 132, 161, 208, 387, 491]	[1, 63, 306, 471, 819]	[1, 308, 351]
	[1, 50, 396, 464, 646]	[1, 390, 1009]
	[1, 7, 126, 269, 837]	[1, 453, 591]
	[1, 235, 596, 693, 781]	[1, 725, 853]
	[1, 181, 217, 686, 903]	[1, 604, 1274]
		[1, 240, 957]
		[1, 123, 721]

3.1.2 Multiclass-OOC Interference Model

In asynchronous K-user CDMA systems, the received signal is the sum of the desired user signal and the signals of the other $K-1$ interfering users each with its own delay time. The time delay offsets are assumed to be a multiple of the chip period, which is known as the chip synchronous scenario that results in the upper bound on the bit error performance [43]. Assuming perfect power balance (i.e. received power of all users is equal), and neglecting other noise sources, such as the thermal noise and shot noise. Also, in our analysis we did not account for the photon counting nature during the photodetection process. Different approaches to account for the photon arrival rate are used in the literature such

as large deviations theory and saddlepoint approximations, [94]-[96]. In what follows we consider only the case of the strict MWML-OOC code set who have, by definition, non-zero shift autocorrelation and crosscorrelation properties bounded by one.

The decision variable at the output of the correlator of the desired user of the $\bar{q}$-th class is evaluated as (see [P1] for details),

$$Z = W_{\bar{q}} b_{0,1,\bar{q}} + \sum_{q=1}^{Q} I_{q\bar{q}} \tag{3.4}$$

$$= W_{\bar{q}} b_{0,1,\bar{q}} + I_{\bar{q}} \tag{3.5}$$

where $I_{\bar{q}}$ is the total MAI from all classes, $b_{0,1,\bar{q}}$ is the zeroth bit of the first user in the $\bar{q}$-th class, and $I_{q\bar{q}}$ is the total interference of users in class q on users in class $\bar{q}$. In the chip synchronous case, each chip position can be occupied by a Mark from the desired and an interfering user with some probability. Therefore, the sum of such possible interference will follow the binomial random variable distribution. Consequently, the MAI $I_{q\bar{q}}$ is binomially distributed with parameters $(K_q, p_{q\bar{q}})$, and $K_q = K_{\bar{q}} - 1$ when $q = \bar{q}$, where $p_{q\bar{q}}$ denotes the probability that a Mark position from a code in class $\bar{q}$ is hit by a Mark from a code in class q and is equal to [P1, Appendix],

$$p_{q\bar{q}} = \frac{W_{\bar{q}} W_q}{2N_q} \tag{3.6}$$

Note that in general $p_{q\bar{q}} \neq p_{\bar{q}q}$. The factor of $1/2$ is included due to the equal probability for a user to send a '1' or a '0' data bit. A special case is the single class which gives $p = W^2/2N_q$ [43]. The multiclass hit probability in (3.6) depends inversely on the length of the interfering classes. Thus, long code classes cause lower interference and shorter code classes cause higher interference.

The moment generating function of the binomially distributed random variables $I_{q\bar{q}}$ is given by [97],

$$M_{I_{q\bar{q}}}(t) = E\left[e^{tI_{q\bar{q}}}\right] = \left((1-p_{q\bar{q}}) + p_{q\bar{q}} e^{t}\right)^{K_q} \tag{3.7}$$

The total multiclass interference ($I_{\bar{q}}$) distribution is the convolution of Q binomial distributions with unequal parameters. Since the random variables $I_{q\bar{q}}$ are independent, then the moment generating function of the total interference can be expressed as,

$$M_{I_{\bar{q}}}(t) = \prod_{q=1}^{Q} M_{I_{q\bar{q}}}(t) \tag{3.8}$$

then the mean of the MAI is,

$$R = \mathbf{E}\left[I_{\bar{q}}\right] = M'_{I_{\bar{q}}}(0) = \sum_{q=1}^{Q} K_q p_{q\bar{q}} \tag{3.9}$$

This is mathematically intractable and a much simpler solution with acceptable accuracy

can be obtained by approximating the binomially distributed interference per class into a Poisson distribution as

$$P_{I_{q\bar{q}}}\left(I_{q\bar{q}}=n\right)\approx\frac{\left(K_q p_{q\bar{q}}\right)^n}{n!}e^{-K_q p_{q\bar{q}}} \tag{3.10}$$

This can be justified by the sparsity of the OOCs which results in low probability of hit and according to the low of rare events. The error incurred due to this approximation is quantified by the following theorem [98].

Theorem 3.1 *Let $\epsilon_1, \epsilon_2, ...$ be independent Bernoulli random variables, where $\Pr\{\epsilon_i = 1\} = p_i$ and $\Pr\{\epsilon_i = 0\} = 1 - p_i$ and let $S_n = \epsilon_1 + ... + \epsilon_n$. The exact probabilities for S_n and Poisson probabilities with parameter $\mu = p_1 + ... + p_n$ differ by at most*

$$|\Pr\{S_n = k\} - \frac{\mu^k e^{-\mu}}{k!}| \leq \sum_{i=1}^{n} p_i^2 \tag{3.11}$$

Proof 3.1 *See* [98], *page 285* .

Therefore, for the q-th class the modeling error is less than $W_q^2/4N_q$ which is small for large N_q and small W_q as is the case in OOCs. For example for an OOC with (1000,7), the modeling error is about 1%. Since the sum of iid Poisson distributed random variables is also Poisson distributed with PMF, then,

$$\begin{aligned} P_{I_{\bar{q}}}\left(I_{\bar{q}}=n\right) &\approx \frac{\left(\sum_{q=1}^{Q} K_q p_{q\bar{q}}\right)^n}{n!}e^{-\sum_{q=1}^{Q} K_q p_{q\bar{q}}} \\ &= \frac{R^n}{n!}e^{-R} \end{aligned} \tag{3.12}$$

3.1.3 Multiclass-OOC BER performance

Using the Poisson model for the MAI, the BER of the multiclass OOC is written as [P1],

$$P(E) \approx \frac{1}{2}\left[1 - e^{-R}\sum_{n=0}^{\mu-1}\frac{R^n}{n!}\right] \tag{3.13}$$

The BER for several multiclass code cases is numerically investigated in [P1] and the results compared to Monte Carlo simulations. Good agreement is shown in the results which confirms our theoretical findings. In Fig. 3.2 a two-class OOC system performance is plotted for both classes with a code length of the low rate class double that of the high rate class, namely $N_1 = 1000$ and $N_2 = 2000$. The code weight of the high rate class is fixed at the value of 5 and the code weight of the low rate class is varied from 4 to 9. It is clear that the performance of one class is better than the other whenever its code weight is higher, with approximately equal performance at the two curves crossing point of 5 (i. e., equal weight). It is noticed that the longer weight class has a slightly higher BER than the shorter code class. This is mainly due to the increased hit probability form shorter codes on longer codes according to (3.6). Although the weight of the high rate class need not to be less than that of the lower rate user classes, but higher weight will limit the number of supported users in the high rate class significantly due to the shorter code length. Finally, the effect of

the code length in one class when fixing all the other parameters is depicted in Fig. 3.3. As the code length of one of the classes increases, its MAI on all the other classes decreases, because of decreasing the probability of hit. Thus, increasing (decreasing) the code length of one class will decrease (increase) the BER of all the other classes in a same proportion.

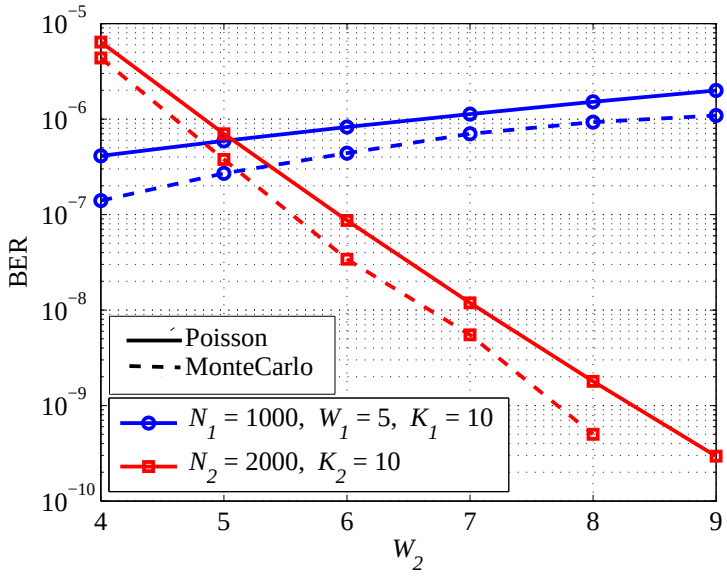

Figure 3.2: Bit error rate for a two-class OOC system as a function of the code weight of the low rate class.

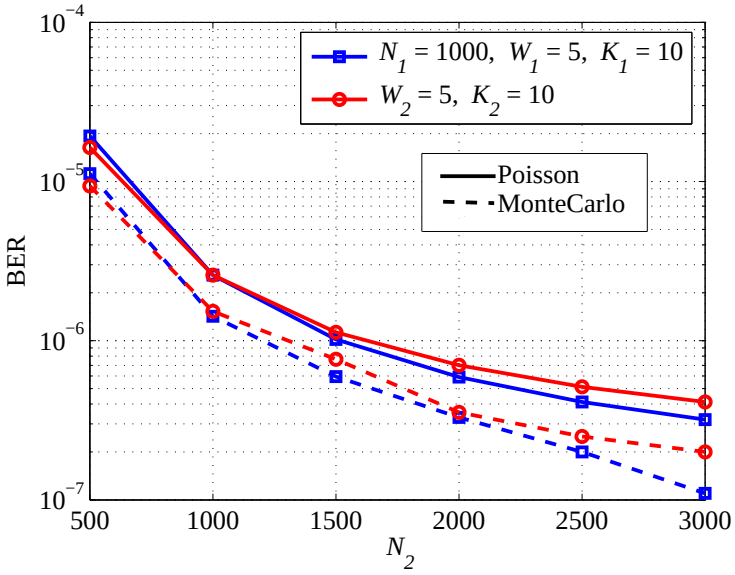

Figure 3.3: Bit error rate for a two-class OOC system as a function of the code length of the second class.

To conclude, we have presented in [P1] a proposal of the construction of a multi-weight, multi-length , strictly orthogonal, optical code set. The code set is flexible because it can be designed for any code lengths and weights limited only by the possible number of codes. Moreover, the code set contains codes with different code lengths and code weights while satisfying the required correlation properties of the strict OOCs. The different code lengths support multirate data services, and the different code weights support data applications with different QoS requirements. By approximating the binomially distributed MAI per class using the Poisson distribution, the analysis of multiclass MAI is simplified significantly. We showed that the multiclass optical orthogonal code performance differentiation is controlled mainly by the code weights. By changing the length of any class, the performance of all classes changes by the same amount. This is a direct consequence of the correlation properties of the strict OOC.

3.2 Polarized-OOC [P2]

The number of users in the original OOC is limited by the requirement that the correlation properties to by bounded by one. If this condition is relaxed then more users can be accommodated but with poorer performance. OOCs with large crosscorrelations are investigated in [46], [99]-[100]. Alternatively, the number of users can be increased by the use another dimension in the coding process such as the polarization of the optical beam while keeping the correlation properties of the constructed code the same as those of the original OOC. In [P2] we proposed the use of the polarized-OOC code which is generated using the MPD set approach. Polarized-OOC cardinality is shown to be two times that of the conventional OOC. Furthermore, since the correlation properties of the Polarized-OOC are the same as of conventional OOC, their error rate performance analysis is similar.

The ability to apply Polarized-OOCs can be justified by the applicability of PolSK . In a Polarized-OOC system the SOP of the pulses is rotated to two orthogonal SOPs $\mathbf{J}_1$ and $\mathbf{J}_2$ in accordance with a given Polarized-OOC code.

The MPD elements can be deduced by considering two consecutive encoded data bits of '1'

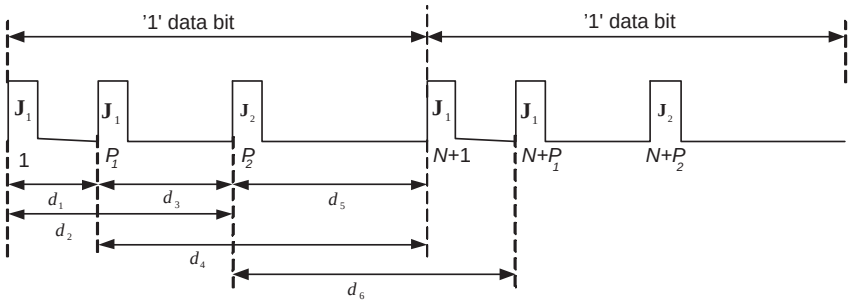

Figure 3.4: Mark positions and differences for a (N,3) polarized-OOC.

as shown in Fig. 3.4. The individual chips are marked with the corresponding Jones vector representing one of a two possible orthogonal SOPs. As we discussed earlier, the position of the W individual chips of the k-th user code is denoted by $c_k = [U_1, U_2, ..., U_W], U_1 = 1$, and in case of polarized-OOC the sign of U_i indicates the SOP. For a positive signed U_i the SOP is $\mathbf{J}_1$ and for a negative signed U_i the SOP is $\mathbf{J}_2$. Then the MPD is given by,

$$d_k = \{\text{sgn}(U_i) \times \text{sgn}(U_j) \left[N - [N + |U_i| - |U_j|]_{mod(N)}\right]\} \tag{3.14}$$

for $i \neq j$ and $i, j = 1, 2, ..., W$; where $\text{sgn}()$ is the sign operator. Now, the possible differences in (3.14) can be only in the set of integer numbers as $\mathbf{D}_{Polarized-OOC} = \{\pm 1, \pm 2, ..., \pm(N-1)\}$. Comparing with (2.12) it is clear that $|\mathbf{D}_{Polarized-OOC}| = 2|\mathbf{D}_{OOC}|$, which leads to doubling of the number of codes. Assuming that we have $K_{Polarized-OOC}$ codes in the Polarized-OOC codeset. Since for each code the MPD length is $W(W-1)$ and the total possible differences is $2(N-1)$ then $K_{Polarized-OOC}W(W-1) \leqslant 2(N-1)$. Therefore, the number of codes in the Polarized-OOC is upper bounded by,

$$K_{Polarized-OOC} \leqslant \left\lfloor \frac{2(N-1)}{W(W-1)} \right\rfloor \tag{3.15}$$

3.2.1 Multiclass Polarized-OOC

The extension of Polarized-OOC to support multiclass users is straightforward. Assume that we have a Q-class system where each class is represented by the length, weight pairs (N_q, W_q) with $N_1 \leq ... \leq N_q ... \leq N_Q$ and the number of users in the q-th class is K_q. Using the algorithm shown in Figure 3.1 with $\mathbf{D} = \{\pm 1, \pm 2, ..., \pm(N_Q - 1)\}$ and $D_q = \{\pm N_{q-1}, ..., \pm(N_q - 1)\} + \Delta_{q-1}$ a multiclass-Polarized-OOC can be generated. Examples of a multiclass-Polarized-OOC code sets are shown in Table 3.2. The multiclass-OOC cardinality upper bound given in (3.1), (3.2), and (3.3) can be extended to multiclass-Polarized-OOC by modifying the constraints to,

$$\frac{\sum_{q=1}^{Q} K_q W_q (W_q - 1)}{2(N_Q - 1)} \leqslant 1 \tag{3.16}$$

and,

$$K_q \leqslant \left\lfloor \frac{2(N_q - N_{q-1}) + |\Delta_{q-1}|}{W_q(W_q - 1)} \right\rfloor \tag{3.17}$$

Table 3.2: Examples of multiclass-Polarized-OOC code sets.

Three-class strict SWML-Polarized-OOC code set.

(550,5)	(930,5)	(1300,5)
$[1,-6,-73,-80,254]$	$[1,330,628,631,863]$	$[1,-286,-456,731,996]$
$[1,117,-366,-538,541]$	$[1,141,227,-513,884]$	$[1,317,-334,-796,-1107]$
$[1,21,-158,-450,538]$	$[1,-279,-298,-464,657]$	$[1,-167,300,872,-945]$
$[1,23,67,158,-238]$	$[1,-162,413,-824,905]$	$[1,-243,-295,1120,-1247]$
$[1,107,-118,348,515]$	$[1,-603,-813,868,-892]$	$[1,-392,711,-726,1200]$
$[1,-30,-113,373,457]$	$[1,72,81,725,748]$	$[1,82,688,-804,930]$
$[1,-165,332,-355,506]$	$[1,22,672,714,-820]$	$[1,-111,157,754,-1118]$
$[1,209,-213,327,-352]$	$[1,368,-433,656,-664]$	$[1,-23,234,-1006,1097]$
	$[1,99,-397,481,836]$	$[1,-93,-1009,1104,1147]$
	$[1,-317,-679,-681,-786]$	$[1,-109,785,-859,1130]$
	$[1,134,345,-614,842]$	$[1,-88,-533,903,-1117]$
	$[1,670,697,-766,800]$	$[1,-2,226,601,1011]$

Three-class strict MWSL-Polarized-OOC code set.

(550,7)	(550,5)	(550,3)
$[1,77,-87,113,-129,-255,336]$	$[1,-31,397,-443,546]$	$[1,156,220]$
$[1,75,196,362,-468,-478,529]$	$[1,29,-254,266,-489]$	$[1,210,501]$
$[1,240,-241,263,-299,-354,504]$	$[1,47,-68,-156,-182]$	$[1,346,547]$
$[1,-134,-155,326,327,343,394]$	$[1,108,-162,-295,-389]$	$[1,179,214]$
$[1,3,55,163,-177,-371,469]$	$[1,-135,-287,-457,-548]$	$[1,116,526]$
$[1,20,-48,-80,-268,386,-455]$	$[1,-114,-450,454,543]$	$[1,-247,479]$
$[1,-199,296,-309,358,-378,401]$	$[1,-26,-113,130,474]$	$[1,143,481]$
$[1,82,-150,-207,-221,-327,521]$	$[1,-137,-227,359,-403]$	$[1,50,233]$
	$[1,45,322,-360,405]$	$[1,64,283]$
	$[1,-30,160,416,456]$	$[1,-281,381]$
	$[1,149,-286,-420,452]$	$[1,-106,146]$
		$[1,-289,304]$
		$[1,-152,498]$
		$[1,404,490]$
		$[1,13,325]$
		$[1,-463,520]$

Three-class strict MWML-Polarized-OOC code set.

(550,7)	(930,5)	(1300,3)
$[1,8,78,320,-335,-369,527]$	$[1,525,-549,-826,-829]$	$[1,154,-479]$
$[1,45,101,105,-245,-431,-548]$	$[1,-63,-117,-494,-603]$	$[1,-334,-796]$
$[1,-75,129,-171,488,533,-543]$	$[1,195,-338,490,-789]$	$[1,382,453]$
$[1,-167,-269,-308,459,-464,534]$	$[1,65,-192,524,-899]$	$[1,30,1103]$
$[1,-5,-42,53,-274,-440,454]$	$[1,271,-439,-642,781]$	$[1,949,1269]$
$[1,66,-85,124,245,-429,457]$	$[1,-195,350,-449,-491]$	$[1,-267,-924]$
$[1,44,152,237,327,349,537]$	$[1,50,249,308,-885]$	$[1,348,-1094]$
$[1,114,-166,-177,217,333,-426]$	$[1,-315,688,-837,925]$	$[1,-336,578]$
	$[1,-26,92,-310,-825]$	$[1,215,265]$
	$[1,359,-402,754,-812]$	$[1,201,869]$
	$[1,-425,653,-691,-851]$	$[1,-279,-289]$
		$[1,260,562]$
		$[1,-277,-350]$
		$[1,403,1093]$
		$[1,682,718]$
		$[1,-689,-998]$
		$[1,-684,-1211]$

Chapter 4

Optical Power Control

In OCDMA, other users accessing the network at the same time as the desired user give rise to an MAI that can be high enough to make the LAN useless. This is specially true for temporal intensity-based optical coding techniques, such as OOCs and Prime codes, where the users' codes are highly correlated and the code weights are small. Furthermore, MAI in OCDMA networks introduces the near-far problem, thus optical power control can be applied to alleviate the problem and enhance the performance and throughput of the network. Other factors affecting the performance of an OCDMA network are shot noise and thermal noise at the receiver. These impairments can be neglected in optical LANs that apply a higher level of transmission power and optical preamplifiers in front of the receivers. Therefore performance of LANs is limited basically by MAI and amplified spontaneous emission (ASE) generated by the optical amplifiers.

Optical power control for OCDMA networks was extensively discussed in [101]-[103]. In [101], optical power control and Time Hopping for multimedia applications using single wavelength was proposed. The approach accommodates to various data rates using only one sequence by changing the time-hopping rate. However, to realize such system an optical selector device that consists of a number of optical hard-limiters is needed. Unfortunately, the optical hard-limiters are not yet mature for field deployment. Power control has also been considered for optical fast frequency hopping CDMA to provide quality of service compatibility by applying variable attenuators [103, 102]. It has been shown that a great improvement in the system capacity is achieved by the power control but the influence of network impairments such as the nonuniform attenuation due to the difference in fiber lengths, and thermal and shot noise were not considered. Disadvantages of this scheme include the need for multi-wavelength transmitters and susceptibility to wavelength-dependent impairments.

In this chapter the optical power control problem for temporal OCDMA is investigated focusing on three main topics. First appling power control to a star network by considering the optical amplifier noise and neglecting the effect of the photodetector nonlinearity (Section 4.1). Also proposing the concept of network partitioning which simplifies the so-

lution and gives more insight to the problem. Distributed algorithms are also applied and network partitioning helps in this case with SIR estimation. In the second case a network with multi-rate users and the feasibility of power control solution is investigated (Section 4.2). In that regard the spectral radius of the network matrix is used as a measure and an algorithm is proposed to enhance the feasibility of power control solution. Finally, the nonlinear relation between the photodetector incident power and the output SIR is considered and an iterative method to solve the nonlinear power control problem is proposed (Section 4.3). The details of these topics are covered in [P3], [P4], and [P5] respectively. The main results are summarized in the following sections.

4.1 Optical Power Control: Optical Pre-amplified Star Network [P3]

Consider the setup shown in Figure 4.1. Each user uses a Laser source modulated and encoded by the supplied user data and a distinct prime code with prime number q. The signal reaches the receiving end after power losses due to OCDMA encoders-decoders, fiber lines, star coupler. We assume that the network nodes are randomly distributed over an area centered at the star coupler and with a radius of $L_{\min} \leqslant r \leqslant L_{\max}$. The length of the fiber connecting the j-th node to the i-th node through the star coupler can be represented by,

$$L_{ij} = L_i^{rx} + L_j^{tx}, \text{ for } i, j = 1, 2, ..., K \tag{4.1}$$

where, L_i^{rx} and L_j^{tx} are the i-th and j-th fiber length from the receiving and transmitting nodes to the coupler respectively.

Optical preamplifiers are applied to compensate for the sever optical power loss. The Amplified Spontaneous Emission (ASE) noise of the optical amplifier *for each polarization mode*

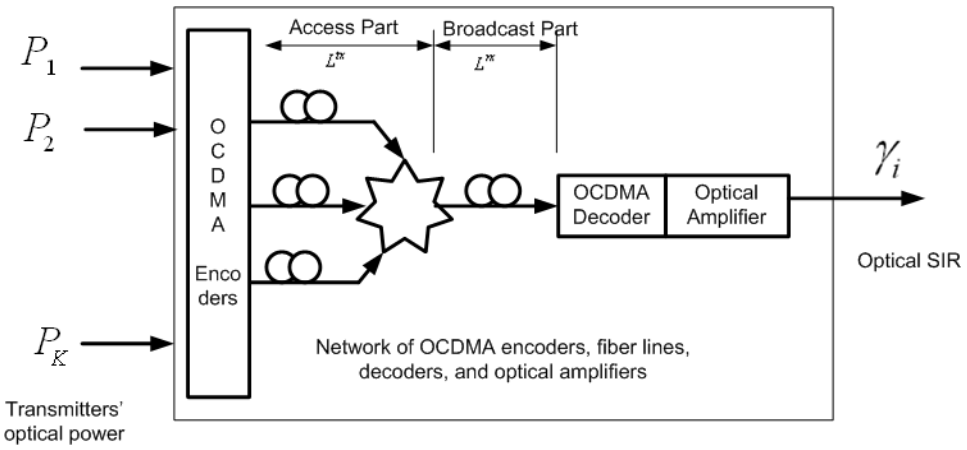

Figure 4.1: An optical CDMA star network with K users.

is given by [18],

$$N_{sp} = n_{sp} h f_c (G_{amp} - 1) B_0 \tag{4.2}$$

where n_{sp} is the spontaneous emission factor typically around 2-5, G_{amp} is the amplifier gain, B_0 is the optical bandwidth, h is Planck's constant, and f_c is the carrier frequency.

4.1.1 Centralized Optical Power Control: Noise-Free

The target carrier to interference power ratio (CIR) required to get a certain QoS as measured by the BER for user i is denoted by Γ_i, which can be different from user to user and the corresponding SIR is denoted by γ_i. Let the transmitted optical power vector be denoted by the k-dimensional column vector $\mathbf{P} = [P_1, P_2, ..., P_k]^T$. Then, optical power control can be considered as an optimization problem by finding the vector $\mathbf{P}$ minimizing the cost function [104],

$$\mathrm{J}(\mathbf{P}) = \mathbf{1}^{\mathrm{T}} \mathbf{P} = \sum_{i=1}^{k} P_i \tag{4.3}$$

Subject to the constraint,

$$\Gamma_i = \frac{P_i G_{ii}}{\sum\limits_{j=1; j \neq i}^{k} P_j G_{ij}} \geqslant \Gamma_{min} \tag{4.4}$$

and

$$0 \leqslant P_i \leqslant P_{\max}; \forall i = 1, ..., k \tag{4.5}$$

where

$\mathbf{1}^{\mathrm{T}} = [1,...,1]$
$k =$ number of active users in the network
$G_{ij} =$ attenuation between transmitting node j and receiving node i including fibers, star coupler and encoders splitting losses
$\Gamma_{min} =$ minimum target carrier to interference power ratio
$P_{\max} =$ maximum transmit optical power

In (4.3) the CIR is at the input of the OCDMA decoder. Optical noise sources such as background radiation can be neglected and only MAI is accounted for. Using matrix form and rearranging terms in (4.4) the optimum power corresponding to the minimum CIR satisfies,

$$[\mathbf{I} - \Gamma_{min} \mathbf{H}] \mathbf{P} = \mathbf{0} \tag{4.6}$$

where $\mathbf{I}$ is the identity matrix and $\mathbf{H}$ is a nonnegative matrix with elements,

$$H_{ij} = \begin{cases} 0 & \text{when } i = j \\ \frac{G_{ij}}{G_{ii}} & \text{when } i \neq j \end{cases} \tag{4.7}$$

$\mathbf{H}$ is called the interference matrix because it quantifies the amount of interference experienced by the desired user due to other users. From linear algebra, a solution to (4.6) exists

only if $1/\Gamma_{min}$ is an eigenvalue of $\mathbf{H}$ and its corresponding positive eigenvector $\mathbf{P}^*$ will be the optimum power vector. According to Perron-Frobenius theorem [105], there exists a positive vector associated to the maximum eigenvalue of the nonnegative and irreducible $k \times k$ matrix $\mathbf{H}$. Therefore, using the CIR constraint in (4.4) the solution of the power control is the eigenvector corresponding to the largest absolute eigenvalue $|\lambda_{max}|$ or the spectral radius $\rho(\mathbf{H})$ of the interference matrix $\mathbf{H}$. Hence, the maximum achievable CIR (target CIR satisfied by all nodes at the same time) is $\Gamma_{max} = 1/|\lambda_{max}|$.

When perfect power control is assumed then the received power from all users is equal at the point of reception. Consequently, taking this into account in (4.4) the maximum achievable CIR (MAI-limited and noise-free) in the optical star network is,

$$\Gamma_{max} = \frac{1}{k-1} \tag{4.8}$$

Therefore, from (4.8) and $\Gamma_{max} = 1/|\lambda_{max}|$, the maximum eigenvalue of the $k \times k$ matrix $\mathbf{H}$ is $k-1$. Which also means that the spectral radius of $\mathbf{H}$ is equal to the number of nodes connected to the network minus one, i.e., $\rho(\mathbf{H}) = k-1$. Furthermore, from (4.8) we conclude that Γ_{max} is limited only by the number of nodes and the network attenuation plays no role in that respect. Assume for instance, that k_1 nodes are switched off and the other $k-k_1$ active nodes power are not changed, then the Γ_{max} will jump to $\frac{1}{k-k_1-1}$.

4.1.2 Centralized Optical Power Control: ASE noise non-negligible

When ASE is much smaller than MAI, the SIR is the processing gain times the CIR. If the ASE is non-negligible, the SIR constraint that account for the noise is used as,

$$\gamma_i = \frac{G_{amp} q^2 P_i G_{ii}}{\sigma^2 G_{amp} \sum\limits_{j=1;j\neq i}^{k} P_j G_{ij} + 2N_{sp}} \geqslant \gamma_{min} \tag{4.9}$$

where the factor of 2 that multiplies the noise term N_{sp} accounts for the two optical polarization modes and σ^2 is the average variance of croscorrelation magnitude given in (2.17). Rearranging terms we get the transmitted optical power for the i-th user,

$$P_i = \frac{\gamma_i \sigma^2}{q^2} \sum_{j=1;j\neq i}^{k} P_j \frac{G_{ij}}{G_{ii}} + \frac{2\gamma_i N_{sp}}{q^2 G_{amp} G_{ii}} \tag{4.10}$$

Equation (4.10) can be written more compactly by defining a scaled SIR and noise power as,

$$\Lambda_i = \frac{\gamma_i \sigma^2}{q^2} \tag{4.11}$$

and

$$u_i = \frac{2\gamma_i N_{sp}}{q^2 G_{amp} G_{ii}} \tag{4.12}$$

Hence in matrix notations we have,

$$[\mathbf{I} - \mathbf{\Lambda H}]\,\mathbf{P} \geqslant \mathbf{u} \tag{4.13}$$

where the matrix $\mathbf{\Lambda}$ is a diagonal matrix with (4.11) as its elements and reduces to a single element if the target SIR of all nodes is the same. Hence, the optimum transmitted power required by all users should be selected to satisfy,

$$\mathbf{P}^* = [\mathbf{I} - \mathbf{\Lambda H}]^{-1}\,\mathbf{u} \tag{4.14}$$

Working at high laser power values is not preferable in optical networks due to restrictions on light sources, fiber nonlinearities and safety requirements. Therefore, whenever a number of active users change their state to the OFF state, the SIR of the remaining active users will increase and a reduction of the corresponding transmitted power according to (4.14) is recommended to get back to the minimum SIR value. An important result of the above analysis is that the SIR theoretical upper bound (MAI-limited and noise-free) in optical CDMA star networks applying prime coding is given by,

$$\gamma_{max} = \frac{q^2}{\sigma^2(k-1)}. \tag{4.15}$$

That is the theoretical upper bound is limited by the number of active users and the supplied code correlation properties.

4.1.3 Centralized Optical Power Control: Network Partitioning

If the optical star network is partitioned into an access part (with j-th link attenuation of g_j) and a broadcast part (with i-th link attenuation of $\hat{g}_i$) as labeled on Figure 4.1. Then, for the noise-free case we can state the following theorem,

Theorem 4.1 *In a MAI-limited (noise-free) star coupled OCDMA network using temporal encoding with code weight q and code cross-correlation variance σ^2, the maximum achievable SIR at the receiving nodes equals the maximum achievable CIR at the star coupler output times a processing gain factor of q^2/σ^2, i.e., the fiber lengths after the star coupler play no role in optimum power evaluation.*

Proof 4.1 *Using $G_{ij} = g_j\hat{g}_i$ in (4.9) we have,*

$$\gamma_i = \frac{G_{amp}q^2P_i}{G_{amp}\sigma^2\sum\limits_{j=1;j\neq i}^{K} P_j\frac{g_j}{g_i} + \frac{2N_{sp}}{g_i\hat{g}_i}} \geqslant \gamma_{min} \tag{4.16}$$

Setting the noise term to zero, and noting that the CIR at the output of the access part of the network is given by,

$$\Gamma_i = \frac{P_ig_i}{\sum\limits_{j=1;j\neq i}^{K} P_jg_j} = \frac{P_i}{\sum\limits_{j=1;j\neq i}^{K} P_j\frac{g_j}{g_i}} \tag{4.17}$$

Therefore, The noise-free SIR at the receiving node can be set using the noise-free CIR at the output

of the star coupler regardless of any attenuation that takes place after the coupler. Furthermore, by using $G_{ij} = g_j \hat{g}_i$ in (4.7) the interference matrix elements are given by,

$$H_{ij} = \begin{cases} 0 & when \ \ i = j. \\ \frac{g_j}{g_i} & when \ \ i \neq j. \end{cases} \tag{4.18}$$

Therefore, it is clear that the fiber cables after the star coupler do not play a role in the MAI encountered by the receiving nodes. The proof is complete.

The result in Theorem 4.1 makes it easier to apply distributed power control algorithms as demonstrated in the following.

4.1.4 Distributed Optical Power Control

The positive side of the centralized algorithm is that it provides the optimum power setting which can be used as a framework to compare other techniques. On the other hand, the main draw back of the centralized algorithm is the need for a central node with all information (network wide) about the link gains and the status of each node. The central node calculates and informs each node of its optimum transmission power. This has to be done whenever a node is switched ON or OFF, or when the node pairing changes. A logical solution is to look for distributed algorithms that use only local information (Estimated CIR or SIR and current power level). The optical power for the i-th node is updated according to,

$$P_i(n+1) = \Psi(P_i(n), \Gamma_i(n)) \tag{4.19}$$

where $\Psi(.)$ is called the inference function. Many techniques applied to wireless links can be applied directly to the optical regime with only a possible difference of how the CIR is estimated. Some of these techniques are listed in [P3, table 1]. In all listed algorithms an estimate of the CIR is required. We propose two methods, the first one can be classified as a semi-distributed method. In this approach, the total received power $P_{rx}(n)$ (signal plus interference) at the desired node is measured (before OCDMA decoder) and sent back over a feedback channel. The sending node i then uses the following formula to estimate the CIR,

$$\tilde{\Gamma}_i(n) = \frac{P_i(n) G_{ii}}{P_{rx}(n) - P_i(n) G_{ii}} \tag{4.20}$$

Since G_{ii} is needed therefore the power control algorithm will not be fully distributed.

In the second technique the CIR is estimated, keeping in mind network partitioning and Theorem 4.1, using,

$$\tilde{\Gamma}_i(n) = \frac{P_i(n) g_i}{P_{star}(n) - P_i(n) g_i} \tag{4.21}$$

where $P_{star}(n) = \sum_{j=1}^{K} P_j(n) g_j$. Therefore, unlike the first method where the total received power at each node is sent back to transmitting nodes, only a single quantity which is the total optical power at the output of the star coupler is reported to all transmitting nodes

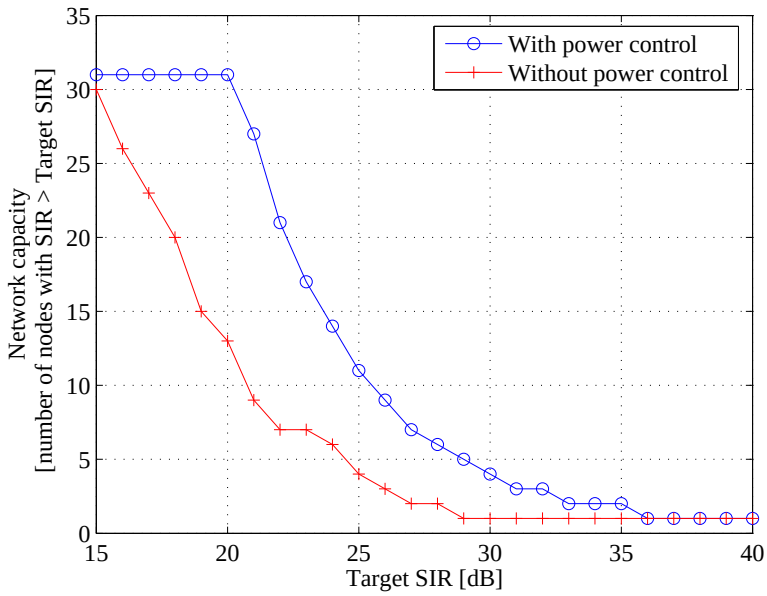

Figure 4.2: Number of supported nodes satisfying the target SIR in a Prime coded network with and without power control. Prime number of 31.

and used in CIR estimation. Hence, the proposed technique in (4.21) is only dependent on local information and the power control algorithms using it will be fully distributed.

Finally, simulation results are given in [P3] to validate our theoretical findings. Figure 4.2 shows a reproduction of the system capacity in terms of number of supported node with or without power control and a significant gain can be noticed. This figure was generated by increasing the size of the network from 1 to 31 for each target SIR value and calculating the size of the network in which all of its nodes can support the target SIR. Therefore, for high target SIR values (> 35 dB) the two cases approach the smallest possible network size with a single user. For target SIR values smaller than 15 dB all users can be supported by both scenarios. But still in the power controlled case lower power values is needed as compared to the non power controlled case were the users transmit at their maximum power.

4.2 Optical Power Control for Multirate Data Traffic [P4]

To adopt the prime code for multi-rate communication, the chip duration is assumed to be fixed and the bit width is changed by a multiple integer of chips. The network supports M-QoS classes and each class has q_i codes generated according to (2.16). And the length of the prime signature sequence of the i-th user is related to the bit and chip durations by $q_i^2 = T_i/T_c$, where T_i is the data bit period of the i-th user and T_c is the chip period. Therefore, nodes with larger q_i correspond to lower data rates that map to a higher SIR in case of back-to-back equal power scenario. The average variance of the cross-correlation

magnitude between the i-th and the j-th prime signature sequences is denoted by σ_{ij}^2 and tabulated in [P4, Table 1] for several primes, noting that $\sigma_{ji}^2 \simeq \sigma_{ij}^2$. It is clear also that for $j = i \pm 1$ the value of σ_{ij}^2 will be significant, consequently the correlation properties of the multirate code will be poor. In this work we concentrate mainly on applying power control concepts to enhance system performance, hence, we adopt the simple multirate coding scheme described above. For more advanced and complex optical prime codes with favorable correlation properties and supporting multimedia traffic see [106].

The use of power control in Section 4.1 for single data rate traffic can be extended to the multirate traffic case. Using,

$$H_{ij} = \begin{cases} 0 \text{ if } i = j \\ \frac{\sigma_{ij}^2 G_{ij}}{G_{ii}} \text{ if } i \neq j \end{cases} \tag{4.22}$$

and $\mathbf{\Lambda}$ whose elements are,

$$\Lambda_i = \frac{\gamma_i}{q_i^2} \tag{4.23}$$

The value of Λ_i is set by γ_i and q_i^2 therefore it contains information about the SIR and data rate requirements and can be considered as an indicator of the QoS level. For a single QoS, $\mathbf{\Lambda}$ matrix is reduced to a single element. Likewise, the elements of the scaled noise vector $\mathbf{u}$ are given by,

$$u_i = \frac{\Lambda_i}{G_{amp} G_{ii}} \sigma_{n,i}^2 \tag{4.24}$$

Then, the optimum power can be evaluated using (4.14).

4.2.1 Spectral Radius Analysis

In a K-node star network where each node can select its rate from a set of Q values and its target SIR from a set of S values, there are $Q^K S^K$ possible SIR-rate combinations. For any combination, the matrix $[\mathbf{I} - \mathbf{\Lambda H}]$ in (4.14) is invertible and positive if,

$$\rho(\mathbf{\Lambda H}) < 1 \tag{4.25}$$

If $\rho(\mathbf{\Lambda H}) \geq 1$ then the system is called infeasible which means that some or all nodes will never be able to achieve their target SIR. In this case one should relax the system QoS requirements to make it feasible by either reducing the target QoS of some nodes, or one or more nodes could be switched off.

To quantify the feasibility of the power control problem solution we investigate the spectral radius in probabilistic terms. Based on extensive numerical simulations, the spectral radius could be modeled as a truncated Gaussian distribution. The mean and variance of this random variable are denoted by $\mathbf{E}[\rho(\mathbf{\Lambda H})]$ and $\mathbf{Var}[\rho(\mathbf{\Lambda H})]$ respectively. Therefore, the probability of feasibility can be evaluated by integrating the truncated Gaussian random

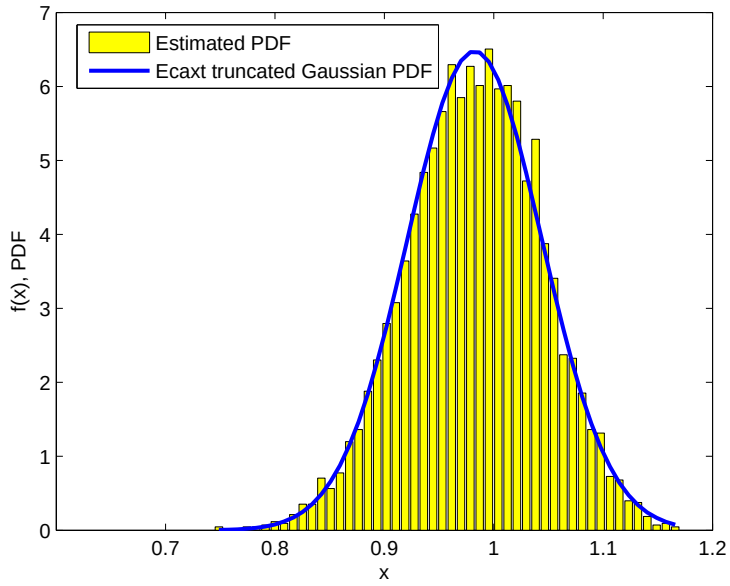

Figure 4.3: Estimated and theoretical PDF of $\rho(\mathbf{\Lambda H})$.

variable from $-\infty$ to 1. Hence, the probability of feasible network is,

$$\mathbf{P}\left[\rho(\mathbf{\Lambda H}) < 1\right] = 1 - Q\left(\frac{1 - \mathbf{E}[\rho(\mathbf{\Lambda H})]}{\sqrt{\mathbf{Var}[\rho(\mathbf{\Lambda H})]}}\right) \tag{4.26}$$

where $Q(x)$ is the integral of the normalized Gaussian function from x to infinity. A scaling factor of the truncated Gaussian (equals $1/Q(-\mathbf{E}[\rho(\mathbf{\Lambda H})]/\mathbf{Var}[\rho(\mathbf{\Lambda H})])$) is neglected because it is approximately unity for $\mathbf{E}[\rho(\mathbf{\Lambda H})]/\mathbf{Var}[\rho(\mathbf{\Lambda H})] > 5$. For typical values used in [P4] we have $\mathbf{E}[\rho(\mathbf{\Lambda H})]/\mathbf{Var}[\rho(\mathbf{\Lambda H})] \gg 5$.

As an example we simulated an optical network with the following parameters. We generated 5000 network realizations and in each realization each user can select its rate, SIR, fiber lengths combination from $q = \{23, 31, 37\}$, 50 to 100, and 2 to 50 km; respectively. For each realization we evaluate $\rho(\mathbf{\Lambda H})$. Also, the mean and variance of the spectral radius is evaluated and their ratio is $\mathbf{E}[\rho(\mathbf{\Lambda H})]/\mathbf{Var}[\rho(\mathbf{\Lambda H})] = 259$ which means that the scaling factor of the truncated gaussian can be neglected. Then a histogram of the result is plotted along with theoretically calculated PDF and a clear agreement is shown in Figure 4.3.

Since there is no closed form expression for the spectral radius $\rho(\mathbf{\Lambda H})$ in (4.26) in terms of the marginal spectral radiuses of $\mathbf{H}$ and $\mathbf{\Lambda}$, therefore, we consider its upper and lower bounds as,

$$\rho(\mathbf{H}) \min(\mathbf{\Lambda}) \leq \rho(\mathbf{\Lambda H}) \leq \rho(\mathbf{H}) \max(\mathbf{\Lambda}) \tag{4.27}$$

Using (4.22) and $\sigma^2 = E\{\sigma_{ij}^2\}$, the spectral radius of $\mathbf{H}$ is equal to $\rho(\mathbf{H}) = \sigma^2(K-1)$. Then,

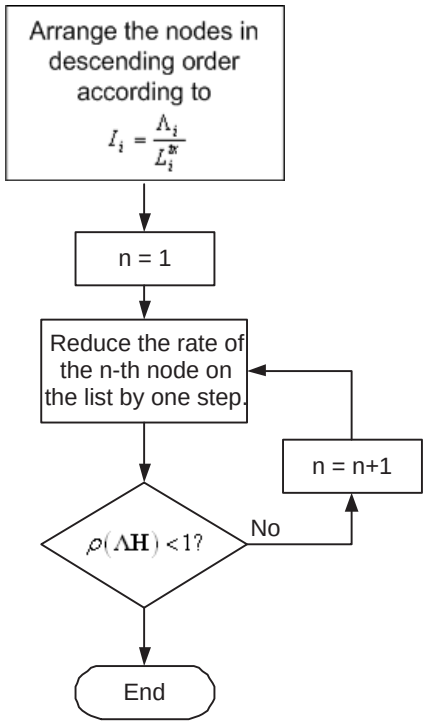

Figure 4.4: Rate-Reduction algorithm.

remembering (4.23) we can write,

$$\sigma^2(K-1)\frac{\gamma_{min}}{q_{max}^2} \leq \rho(\mathbf{\Lambda H}) \leq \sigma^2(K-1)\frac{\gamma_{max}}{q_{min}^2} \tag{4.28}$$

where $\gamma_{min}, \gamma_{max}, q_{min}^2$ and q_{max}^2 are the minimum target SIR, maximum target SIR, minimum code length (proportional to maximum rate), and maximum code length (proportional to minimum rate), respectively. Consequently, the designed network QoS is guaranteed if the maximum allowable SIR and the minimum code length are selected to satisfy,

$$\gamma_{max} < \frac{q_{min}^2}{\sigma^2(K-1)} \tag{4.29}$$

4.2.2 Rate reduction algorithm

If the condition in (4.29) is met, then the QoS of all users will be satisfied. This leads to inefficient usage of network resources since the upper bound is far from the actual values of the spectral radius. Hence, we consider the case when the guaranteed feasibility condition (4.25) is violated and study the CDF of the relating spectral radius for the various QoS levels. Under certain QoS requirements the network will be in the outage condition, i.e., the spectral radius is greater than one and the target QoSs cannot be met using power control. Therefore, we apply a removal algorithm to improve system feasibility. Instead

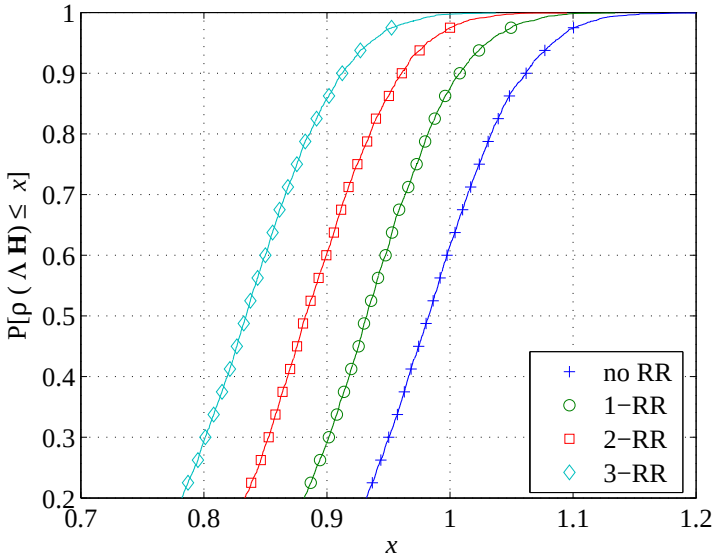

Figure 4.5: CDF of spectral radius with different RRs.

of switching off some nodes completely we propose a removal algorithm that keeps all the nodes on but with reduced data rate. We call this algorithm as the Rate Reduction (RR) algorithm. The RR algorithm can be categorized according to the number of nodes k subject to reducing their rate as $k-$RR. Therefore, 1-RR means that only one node is subject to rate reduction, 2-RR refers to rate reduction in two nodes, and so on. We use an indicator variable to select the candidate nodes subject to k-RR as,

$$I_i = \frac{\Lambda_i}{L_i^{tx}} \tag{4.30}$$

Therefore, the indicator variable is maximum for nodes with the highest QoS requirement and shortest fibers from the star coupler, since these nodes are expected to cause the highest interference in the network. If the rate of the nodes with the highest indicators are reduced, then the upper bound in (4.28) decreases. Consequently, the mean and variance of the truncated Gaussian spectral radius will be decreased leading to increased probability of feasibility according to (4.26). A flowchart of the proposed technique is shown in Figure 4.4. The main disadvantage of the proposed k-RR algorithm is that it is a centralized algorithm. Finally, a numerical simulation of the proposed technique was conducted

in [P4] and reproduced here for quick referencing. We generated 10^4 network realizations from which we calculated the CDF of the spectral radius for the Rate Reduction Algorithm. For the applied network parameters, the mean and variance of the network spectral radius are found to be 0.98 and .0036 respectively. Using (4.26) then it is found that, when no RR is applied, around 62% of the time the QoS network requirements can be fulfilled. The same can be deduced from Fig. 4.5 which indicates the validity of the truncated Gaussian

assumption. The network feasibility is increased to around 87%, 97%, and 99% using the 1-RR, 2-RR and 3-RR, respectively. Hence, by using a 3-RR algorithm one can find a feasible network for 99 % of the time.

4.3 Optical Nonlinear Power Control (ONPC) [P5]

The work in previous sections assumes the use of optical preamplifiers with the ASE as the noise source and neglecting the effect of photodetection. In this section we consider the effect of the photodetection nonlinearity on the power control solution without optical preamplifiers. We relate the SIR after the photodetector to the incident optical power due to the desired and MAI signals. Then we seek to solve for the optimum transmit power setting that result in satisfying the required target SIR values. In this case we have two major differences compared to the conventional power control. First, the SIR value is related to the square of the users' transmit power. Consequently, linear solution to the problem can not be applied and an iterative method is proposed. Second, the photodetector shot noise creates a self interference term which is not considered in the conventional power control as part of the MAI. Therefore, increasing the transmit power of any user is not always beneficial for selfish users.

The noise at the photodetector output is given by,

$$N_i = \sigma_t^2 + \sigma_{s,i}^2 \tag{4.31}$$

where σ_t^2 is the thermal noise power given by,

$$\sigma_t^2 = \frac{4k_B T}{R_L} F_n B \tag{4.32}$$

and $\sigma_{s,i}^2$ is the shot noise power given by,

$$\sigma_{s,i}^2 = 2e\Re B P_{r,i} \tag{4.33}$$

where B[Hz] is the receiver noise equivalent bandwidth. In (4.32) and (4.33), e denotes the electron's charge, and k_B is the Boltzmann's constant. We assume some typical parameters for the noise figure of F_n to 3 [dB], temperature to T= 300^o[K], the load resistance R_L to 100 Ω, and photodiode's responsitivity $\Re$ to 1.25 [A/W]. Hence, the Signal to Interference Ratio (SIR) at the photodetector output can be defined as,

$$\gamma_i = \frac{\left(\Re W^2 P_i G_{ii}\right)^2}{\Re^2 \alpha^2 \left(\sum_{j \neq i} P_j G_{ij}\right)^2 + N_i} \tag{4.34}$$

Then, expanding (4.34) using (4.32) and (4.33) and defining $I_i = \sum_{j \neq i} P_j G_{ij}$ as the MAI and

$\mu = 2e\Re B$ we get,

$$\gamma_i = \frac{\left(\Re W^2 P_i G_{ii}\right)^2}{\Re^2 \alpha^2 I_i^2 + \mu\alpha I_i + \mu W^2 P_i G_{ii} + \sigma_t^2} \tag{4.35}$$

It can be seen that the SIR depends inversely on the square of MAI (first term in the denominator) due to the nonlinearity in the detection process. Similarly, the SIR depends inversely on the linear summation of optical power from all users due to the shot noise term; therefore, each user will suffer a self interference which will be high for short range (G_{ii} in the denominator is large) low data rate nodes if no power control is applied. In [P5] we solved (4.35) and the power update procedure is found to be,

$$P_i = \Gamma_i \left(1 + \sqrt{1 + \lambda_i}\right) \tag{4.36}$$

where,

$$\Gamma_i = \frac{\mu\gamma_i}{2\Re^2 W^2 G_{ii}}, \tag{4.37}$$

and,

$$\lambda_i = \frac{4}{\mu^2 \gamma_i}\left[\Re^4 \alpha^2 I_i^2 + \mu\Re^2 \alpha I_i + \Re^2 \sigma_t^2\right] \tag{4.38}$$

$$= K_1 I_i^2 + K_2 I_i + K_3 \tag{4.39}$$

From (4.36) it is clear that the power update for the i-th user depends on the power level of all other users, i.e., on the MAI. Therefore, we can write (4.36) as a set of nonlinear equations as,

$$P_i = f_i(\mathbf{P}), \quad i = 1, 2, ..., K \tag{4.40}$$

where $\mathbf{P} = [P_1, P_2, \cdots, P_K]^T$ is the transmitted power vector. The power control is defined in this setup by a set of second order equations. The convergence analysis of this algorithm is given in the next section.

4.3.1 Convergence Analysis of the ONPC Algorithm

Equation (4.40) is in form of fixed point iteration, and the optimum power control values can be found iteratively as,

$$P_i\left(t+1\right) = f_i\left(\mathbf{P}\left(t\right)\right), \ \forall i = 1, \cdots, K \tag{4.41}$$

or in a vector form,

$$\mathbf{P}\left(t+1\right) = \mathbf{F}\left(\mathbf{P}\left(t\right)\right), \tag{4.42}$$

where

$$\mathbf{F}\left(\mathbf{P}\left(t\right)\right) = \left[f_1\left(\mathbf{P}\left(t\right)\right), \cdots, f_N\left(\mathbf{P}\left(t\right)\right)\right]'$$

The convergence of the iterative power control algorithm is investigated in light of theory of standard interference function [107]. The interference function $\mathbf{F}(\bullet)$ is called standard when the following properties are satisfied for all the components of the nonnegative

power vector $\mathbf{P}$:

- Positivity: $\mathbf{F}(\mathbf{P}) > 0$;
- Monotonicity: if $\mathbf{P} \geq \mathbf{V}$ then $\mathbf{F}(\mathbf{P}) \geq \mathbf{F}(\mathbf{V}) > 0$;
- Scalability: for all $\varepsilon > 1$, $\varepsilon\mathbf{F}(\mathbf{P}) > \mathbf{F}(\varepsilon\mathbf{P})$.

The following theorems are valid for the Standard Interference Functions [107]:

Theorem 4.2 *If the standard power control algorithm has a fixed point, then that fixed point is unique.*

Proof 4.2 *See [107].*

Theorem 4.3 *If **F(P)** is feasible, then for any initial power vector $\boldsymbol{P}(0)$, the standard power control algorithm converges to a unique fixed point $\mathbf{P}^*$.*

Proof 4.3 *See [107].*

Theorem 4.4 *If **F(P)** is feasible, then from any initial power vector $\boldsymbol{P}(0)$, the asynchronous standard power control algorithm converges to a unique fixed point $\mathbf{P}^*$.*

Proof 4.4 *See [107].*

Based on the previous theorems we can introduce the following proposition:

Proposition 4.1 *For any **P(0)**, the ONPC algorithm (4.36)-(4.40) will always converge to a unique fixed point $\mathbf{P}^*$.*

Proof 4.5 *We will prove that the ONPC algorithm is a standard power control algorithm. We start with the following observations*

(a) $I_i(\boldsymbol{P}) = \sum_{j \neq i} P_j G_{ij} \geq 0$.

(b) If $\boldsymbol{P} \geq \boldsymbol{V}$, *then* $I_i(\boldsymbol{P}) \geq I_i(\boldsymbol{V})$.

(c) For any real scalar ε, $I_i(\varepsilon\boldsymbol{P}) = \sum_{j \neq i} \varepsilon P_j G_{ij} = \varepsilon I_i(\boldsymbol{P})$.

Then,

1. *Positivity:* $\mathbf{P} \geqslant 0,\ \mathbf{F}(\mathbf{P}) \geqslant \mathbf{0}$
   $f_i(\mathbf{P}) = \Gamma_i \left(1 + \sqrt{1 + K_1 I_i^2 + K_2 I_i + K_3}\right)$,
   $\because \Gamma_i \geqslant 0,\ K_1 \geqslant 0,\ K_2 \geqslant 0,\ K_3 \geqslant 0$, *and from (a)* $I_i(\mathbf{P}) \geqslant 0$
   then $f_i(\mathbf{P}) \geqslant 0\ \forall i$
2. *Monotonicity: Let* $\mathbf{P} \geqslant \mathbf{V} \geqslant \mathbf{0}$,
   Let $\mathbf{P} = \mathbf{V} + \mathbf{B} \Rightarrow f_i(\mathbf{P}) = \Gamma_i \left(1 + \sqrt{1 + K_1 I_i^2(\mathbf{P}) + K_2 I_i(\mathbf{P}) + K_3}\right)$
   $= \Gamma_i \left(1 + \sqrt{1 + K_1 I_i^2(\mathbf{V} + \mathbf{B}) + K_2 I_i(\mathbf{V} + \mathbf{B}) + K_3}\right)$
   $I_i^2(\mathbf{V} + \mathbf{B}) \geqslant I_i^2(\mathbf{V}) + I_i^2(\mathbf{B})$

$$\Rightarrow f_i(\mathbf{P}) \geqslant \Gamma_i\left(1+\sqrt{1+K_1I_i^2(\mathbf{V})+K_1I_i^2(\mathbf{B})+K_2I_i(\mathbf{V})+K_2I_i(\mathbf{B})+K_3}\right)$$
since $I_i(\mathbf{B}) \geqslant 0$,
$$f_i(\mathbf{P}) \geqslant \Gamma_i\left(1+\sqrt{1+K_1I_i^2(\mathbf{V})+K_1I_i^2(\mathbf{B})+K_2I_i(\mathbf{V})+K_2I_i(\mathbf{B})+K_3}\right) \geqslant$$
$$\Gamma_i\left(1+\sqrt{1+K_1I_i^2(\mathbf{V})+K_2I_i(\mathbf{V})+K_3}\right) = f_i(\mathbf{V})\,\forall i$$

3. *Scalability: Let* ε *is scalar and greater than one* ($\varepsilon > 1$)*:*
$$\varepsilon f_i(\mathbf{P}) = \varepsilon\Gamma_i\left(1+\sqrt{1+K_1I_i^2(\mathbf{P})+K_2I_i(\mathbf{P})+K_3}\right)$$
$$= \varepsilon\Gamma_i + \Gamma_i\sqrt{\varepsilon^2+\varepsilon^2K_1I_i^2(\mathbf{P})+\varepsilon^2K_2I_i(\mathbf{P})+\varepsilon^2K_3}$$
$$> \Gamma_i + \Gamma_i\sqrt{\varepsilon^2+\varepsilon^2K_1I_i^2(\mathbf{P})+\varepsilon^2K_2I_i(\mathbf{P})+\varepsilon^2K_3}$$
$$> \Gamma_i + \Gamma_i\sqrt{1+\varepsilon^2K_1I_i^2(\mathbf{P})+\varepsilon K_2I_i(\mathbf{P})+K_3} = f_i(\varepsilon\mathbf{P})\,\forall i$$

Therefore, the ONPC algorithm is a standard interference function and will converge to a unique point.

4.3.2 ONPC Feasibility

According to Proposition 4.1, the ONPC converges to a unique solution but it is not clear if that unique point satisfies the target SIR requirements, i.e., if there is a feasible solution. The solution feasibility for the iterative procedure in (4.41) can be analyzed using the $\mathbf{D}$ matrix defined as [104],

$$\mathbf{D} = [d_{ij}] = \left[\frac{\partial f_i}{\partial P_j}\right] \tag{4.43}$$

Then using (4.36)-(4.39), and the chain rule we get,

$$d_{ij} = \begin{cases} 0 & \text{if } i = j \\ \frac{1}{2}\Gamma_i(2K_1I_i+K_2)(1+\lambda_i)^{-1/2}G_{ij} & \text{if } i \neq j \end{cases} \tag{4.44}$$

It is well known that, [108], if the spectral radius of the matrix $\mathbf{D}$ is less than one, i.e., $\rho(\mathbf{D}) < 1$, then the map in (4.41) is a contracting map and therefore converges to a fixed point. Note that the elements of the $\mathbf{D}$ matrix in (4.44) are not fixed, but they depend on the level of the MAI.

Proposition 4.2 *If the solution of the ONPC algorithm is feasible, then, for lower levels of MAI the ONPC converges to the solution faster.*

Proof 4.6 *Since for any positive power vector the MAI is also positive and since for any two power vectors such that* $\mathbf{P}_1 > \mathbf{P}_2$ *we have the corresponding two MAI interference vectors* $\mathbf{I}_1 > \mathbf{I}_2$ *where* $\mathbf{P}_1, \mathbf{P}_2, \mathbf{I} \in \Re^N$*. Hence, using (4.44) we have* $\mathbf{D}_1 > \mathbf{D}_2$*. Furthermore, since for any positive matrices such that* $\mathbf{D}_1 > \mathbf{D}_2$ *we have* $\rho(\mathbf{D}_1) > \rho(\mathbf{D}_2)$ *and since the speed of convergence is higher for lower spectral radiuses, then the proof is complete.*

Simulation results of the ONPC can be found in [P5]. In Figure 4.6 an alternative is shown where a target SIR is changed continuously and the actual SIR is plotted for the far-node

and close-node. It is clear that the algorithm converges to a fixed point but in some cases (time epoch 40 to 78) when the target SIR is higher than the maximum achievable, therefore, the spectral radius of the **D** matrix is higher than one an the solution is infeasible.

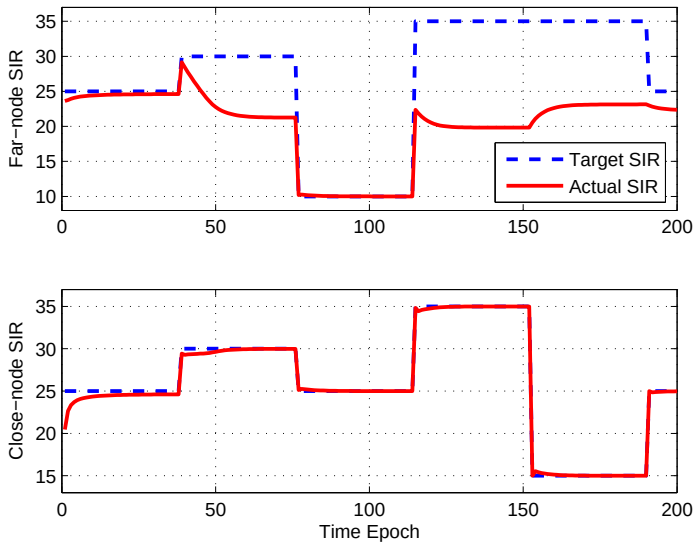

Figure 4.6: Target and actual SIR variations of the far and close nodes.

Chapter 5

Conclusions

5.1 Thesis results

In this thesis three main topics related to optical CDMA were covered. Firstly, OOCs are extended to support multirate traffic data and also polarization domain is used to double the number of supported users. Secondly, power control is investigated to overcome the MAI induced near-far effect. Thirdly, polarization-encoding is proposed as a new method of optical CDMA.

The mark position difference set approach was used to generate multiclass-OOCs, polarized-OOC, and multiclass-polarized-OOCs. This approach is flexible and gives a simplified way of upper bounding the number of codes in the code set. The mark position difference approach simplifies the generation of OOC code sets with arbitrary length and weight that satisfying the desired correlation properties. This is beneficial in systems supporting multimedia applications with different data rates and quality of service. Codes with higher weight give better quality of service, while longer codes support lower data rates. Furthermore, the binomially distributed interference was approximated by Poisson variable which significantly simplified BER evaluation for the multiclass code with acceptable accuracy. Since the number of codes in conventional OOCs is small, the Polarized-OOC was proposed. The Polarized-OOC is the same as the OOC with added optical polarizers and polarization rotators in the branches of the parallel optical delay line encoder. Each mark position in the Polarized-OOC is polarization rotated to two orthogonal states. This approach doubles the upper bound on the OOC code cardinality. The important feature is that only slow polarization control at the receiver is needed. On the other hand, random polarization drifts during transmission through the optical fiber is expected to have minimal effect, as these drifts will be common to all chips in the coded data.

Optical CDMA is an interference limited system, thus, measure should be taken to reduce the effect of the MAI. In optical star networks the variance of the user distances from the star coupler can be significant causing the close users to overpower the far users. Also,

lower rate users with higher code weights will have higher processing gains. Power control was proposed to balance the power for all users in such a way that the SIR at each node is equal. The well-known centralized power control algorithm was considered for optical star networks using prime codes. To simplify, only the fiber attenuation was considered. Dispersion and non-linear effects were neglected. It has been shown that by using the optimum transmit power levels, the quality of service of the users could be made equal. Also it has been shown that, in the noiseless case, the only parameters needed to find the optimum power are the fiber attenuations from the transmitting nodes to the coupler.

By relating the output SIR to the received optical power the SIR will depend nonlinearly on the MAI. Based on this observation the use of a nonlinear iterative power control algorithm was proposed. Convergence analysis also was given and the visibility of solution was investigated. The case of multiclass traffic was also considered under the power control theme. We proposed the use of an algorithm to enhance the feasibility of the power control solution. The algorithm is based on reducing the rate of the nodes with the highest effect on the network.

The use of the SOP for OCDMA networks is proposed and investigated briefly in this work. The SOP of the optical beam is alternated between two orthogonal SOPs according to a given code. We used simulations to demonstrate the effectiveness of the proposed technique.

5.2 Future Work

The author feels that more work is needed on many areas to make possible the production of commercial and cost effective OCDMA systems. On the coding topic, intelligent code design and construction that reduce or eliminate the effect of MAI and can support higher number of users is still an open area. Multi-dimensional codes that use wavelength and time dimensions can be considered to increase the throughput of optical systems. On the other hand, efficient and cost effective optical CDMA encoders and decoders are needed. Integrated optics can be considered to provide the required efficiency. The availability of such devices will significantly enhance the performance of OCDMA and make it more competitive with the well-developed WDM systems.

Existing OCDMA schemes suffer from several disadvantages such as, the required fast optical pulse generation in temporal OCDMA to allow the accommodation of more users, the requirement of high number of multi-wavelength transmitters and susceptibility to wavelength-dependent impairments in frequency-hopping OCDMA, the high multi-user interference effects in spectral encoding OCDMA. On the other hand, two-dimensional incoherent OCDMA is being widely studied due to its robust performance, flexibility of bandwidth provisioning, and use of standard commercial-off-the-shelf technologies. In addition, it shows a high degree of robustness to amplification and transmission effects in fiber since the codes are not phase sensitive. A future study is required that combine

short code length temporal OCDMA, spectral (phase or amplitude) encoding OCDMA, wavelength, and/or polarization spreading to generate a multidimensional OCDMA signal with expected favorable performance. It is expected that the system capacity in terms of number of simultaneous users will be enhanced. Furthermore, the data rate of each individual user could be increased giving rise to increased total system throughput and spectral efficiency. Joining the different OCDMA schemes will require the design of new codes keeping in mind the limitations of each scheme.

The effect of optical fiber channel impairments such as, dispersion, non-linear interactions need to be quantified for accurate judgment of the link performance. Noise mechanisms, such as thermal noise and shot noise should be considered for long fiber spans. On the other hand, the dominating effect of multi-user interference should be characterized. Solutions such as the use optical multi-user detectors, optical power control can also be considered.

Bibliography

[1] Govind P. Agrawal. *Fiber-Optic Communications Systems*. John Wiley & Sons, 2002.

[2] B. Mukherjee G. Kramer and A. Maislos. Etherenet Passive Optical Network (EPON): a missing link in an end-to-end optical internet. *S. Dixit, Ed. New York, Wiley*, Mar. 2003.

[3] S. Dixit C.M. Assi, Y. Ye and M.A. Ali. Dynamic Bandwidth Allocation for Quality-of-Service Over Ethernet PONs. *IEEE J. on Selected Areas in Communications*, Vol. 21:pp: 1467–1477, November 2003.

[4] Glen Kramer. *Ethernet Passive Optical Networks*. McGraw-Hill, 2005.

[5] M.S. Borella, J.P. Jue, D. Banerjee, B. Ramamurthy, and B. Mukherjee. Optical components for wdm lightwave networks. *Proceedings of the IEEE*, Vol. 85:pp: 1274 – 1307, August 1997.

[6] Cisco Systems. Introduction to dwdm for metropolitan networks. *Cisco Systems, Inc.*, pages availabel online at www.cisco.com, last accessed 10.10.2006, June 2001.

[7] T.-P. Lee and C.-E. Zah. Wavelength-tunable and single-frequency lasers for photonic communications networks. *IEEE Commun. Mag.*, Vol. 27:pp: 42–52, Oct. 1989.

[8] et al. T.-P. Lee. Multi wavelength dfb laser array transmitters for ontc reconfigurable optical network testbed. *IEEE/OSA J. Lightwave Technol.*, Vol. 14:pp: 967–976, June 1996.

[9] H. Kobrinski and K.-W. Cheung. Wavelength-tunable optical filters: Applications and technologies. *IEEE Commun. Mag.*, Vol. 32:pp: 50 – 54, Dec. 1994.

[10] J. E. Baron K.-W. Cheung, D. A. Smith and B. L. Heffner. Multiple channel operation of an integrated acousto-optic tunable filter. *Electron. Lett.*, Vol. 25:pp: 375–376, 1989.

[11] A. Sneh and K. M. Johnson. High-speed tunable liquid crystal optical filter for wdm systems. *Proc. IEEE/LEOS'94 Summer Topical Meetings on Optical Networks and Their Enabling Technologies Lake Tahoe, NV*, pages pp: 59–60, July 1994.

[12] M. Ito M. Inai Y. Hattori A. Inoue, M. Shigehara and T. Mizunami. Fabrication and application of fiber bragg gratinga review. *Optoelectron. Devices Technol.*, Vol. 10:pp: 119–130, Mar. 1995.

[13] P. R. Morkel M. Tachibana, R. I. Laming and D. N. Payne. Erbium-doped fiber amplifier with flattened gain spectrum. *IEEE Photon. Technol. Lett.*, Vol. 3:pp: 118–120, Feb. 1991.

[14] A. R. Chraplyvy Forghieri, R. W. Tkach and D. Marcuse. Reduction of four-wave mixing crosstalk in wdm systems using unequally spaced channels. *IEEE Photon. Technol. Lett.*, Vol. 6:pp: 754–756, 1994.

[15] C. A. Brackett. Dense wavelength division multiplexing networks: Principle and applications. *IEEE J. Select. Areas Commun.*, Vol. 8:pp: 948–964, Aug. 1990.

[16] H. S. Hinton. Photonic switching fabrics. *IEEE Commun. Mag.*, Vol. 28:pp: 71–89, Apr. 1990.

[17] Harry G. Perros. *Connection-oriented networks : SONET/SDH, ATM, MPLS, and optical networks*. John Wiley & Sons, 2005.

[18] R. Ramaswami and K.N. Sivarajan. *Optical Networks, a practical perspective*. Morgan Kaufmann, 1998.

[19] B. Mukherjee S. Yao and S. Dixit. Advances in photonic packet switching: An overview. *IEEE Commun. Mag.*, Vol. 38:pp: 84–94, Feb. 2000.

[20] G. Eisenstein R.S. Tucker and S.K. Korotky. Optical time-division multiplexing for very high bit-rate transmission. *Journal of Lightwave Technology*, Vol. 6:1737–1749, November 1988.

[21] N. Karafolas and D. Uttamchandani. Optical fiber code division multiple access networks: A review. *Optical Fiber Technology*, Vol. 2:pp: 149 – 168, 1996.

[22] R. Dixon. Spread spectrum systems,. *WileyŰInterscience, New York.*

[23] R. Scholtz. The spread spectrum concept. *IEEE Trans. Commun.*, Vol. 25:748, no.8.

[24] A. Stok and E.H. Sargent. Lighting the local area: Optical code-division multiple-access and quality of service provisioning. *IEEE Network*, Vol. 14:42–46, November/December 2000.

[25] M.E. Marhic. Coherent optical cdma networks. *Journal of Lightwave Technology*, Vol. 11:pp: 854–864, May/June 1993.

[26] J.P. Heritage J.A. Salehi, A.M. Weiner. Coherent ultrashort light pulse code-division multiple access communication systems. *Journal of Lightwave Technology*, Vol. 8:478–491, March 1990.

[27] R.A. Griffin D.D. Sampson, G.J. Pendock. Photonic code-division multiple-access communications. *Fiber and Integrated Optics*, Vol. 16:129, 1997.

[28] O.K. Tonguz and K.A. Falcone. Fiber-optic interconnection of local area networks: Physical limitations of topologies. *Journal of Lightwave Technology*, Vol. 11:1040–1052, May/June 1993.

[29] T. Ohtsuki. Direct-detection optical asynchronous cdma systems with double optical hard-limiters: Apd noise and thermal noise. *IEICE Trans. Comm.*, Vol. E81-B, July 1998.

[30] H. Sawagashira, K. Kamakura, T. Ohtsuki, and I. Sasase. Direct- detection optical synchronous cdma systems with interference canceller using group information. *IEICE Trans. Fundamentals*, Vol. E83-A, Nov. 2000.

[31] S. Zahedi and J. Salehi. Analytical comparision of various fiber-optic cdma receiver structures. *J. Lightwave Technol.*, Vol. 18:10718, Dec. 2000.

[32] L.A. Rusch H. Fathallah and S. Larochelle. Optical frequency-hop multiple access communications system. *ICC 98. IEEE International Conference on Communications*, Vol. 3:pp: 1269–1273, June 1998.

[33] L.A. Rusch H. Fathallah and S. Larochelle. Passive optical fast frequency-hop cdma communication system. *J. Lightwave Technol.*, Vol. 17:397, March 1999.

[34] L. Bin. One-coincidence sequences with specified distance between adjacent symbols for frequency-hopping multiple access. *IEEE Trans. on Comm.*, Vol. 45:pp: 408–410, 1997.

[35] C.C. Chang, H.P. Sardesai, and A.M. Weiner. Code-division multiple-access encoding and deconding of femtosecond optical pulses over a 2.5-km fiber link. *IEEE Photonics Tech. Let.*, Vol. 10:pp: 171–173, Jan. 1998.

[36] A.M. Weiner. Femtosecond optical pulse shaping and processing. *Progr. Quantum Electron.*, Vol. 3:161, Sept. 1995.

[37] Zaccarin and M. Kavehard. An optical cdma system based on spectral encoding of led. *IEEE Photonics Technology Letters*, Vol. 4:479, April 1993.

[38] M. Kavehard and D. Zaccarin. Optical code-division multiplexed systems based on spectral encoding of noncoherent sources. *J. Lightwave Technology*, Vol. 13:534, March 1995.

[39] K. Iversen and O. Ziemann. An all-optical cdma communication network by spectral encoding of led using acoustically tunable optical filters. *Proc. 1995 Int. Symposium on Signals, Systems and Electronics (ISSSE'95)*, Vol. 18:529, San Francisco 1995.

[40] B. Aazhang L. Nguyen, T. Dennis and J.F. Young. Experimental demonstration of bipolar codes for optical spectral amplitude cdma communication. *J. Lightwave Tech.*, Vol. 15:1647, Sept. 1997.

[41] P.R. Prucnal W.C. Kwong, P.A. Perrier. Synchronous versus asynchronous cdma for fiber-optic lans using optical signal processing. *Global Telecommunications Conference GLOBECOM '89*, Vol. 2:pp: 1012 – 1016, 27-30 Nov. 1989.

[42] J. G. Zhang and G. Picchi. Tunable prime code encoder/decoder for all-optical cdma applications. *Elect. Letters*, Vol. 29:1211–1212, 1993.

[43] J.A. Salehi. Code division multiple access techniques in optical fiber networks-part i: Fundamental concepts. *IEEE Trans. Comm*, Vol. 37:824–833, August 1989.

[44] J. Salehi and C. Brackett. Code division multiple access techniques in optical fiber networks-part ii: Systems performance analysis. *IEEE Trans. Comm*, Vol. 37:834, August 1989.

[45] F.R.K Chung, J.A. Salehi, , and V.K. WEI. Optical orthogonal codes: Design, analysis, and applications. *IEEE Trans. Information Theory*, Vol. 35:pp: 595–604, May 1989.

[46] G. C. Yang and T. E. Fuja. Optical orthogonal codes with unequal auto- and cross-correlations. *IEEE Trans. Inf. Theory*, Vol. 41:pp: 96–106, Jan. 1995.

[47] J. Yin. Some combinatorial constructions for optical orthogonal codes. *Discr. Math.*, Vol. 185:pp: 201–219, 1998.

[48] Y. Miao R. Fuji-Hara and J. Yin. Optimal (9v,4,1) optical orthogonal codes. *SIAM J. Discr. Math.*, Vol. 14:pp: 256–266, 2001.

[49] R. Fuji-Hara Y. Chang and Y. Miao. Combinatorial construction of optimal optical orthogonal codes with weight 4. *IEEE Trans. Inf. Theory*, Vol. 49:pp: 1283–1292, May 2003.

[50] P. R. Prucnal, M. A. Santoro, and T. R. Fan. Spread spectrum fiber-optic local area network using optical processing. *Journal of Lightwave Technology*, Vol. 4:547 – 554, May 1986.

[51] P. R. Prucnal. Vlsi fiber optic local area network. *SPIE Proc.*, Vol. 700:230, 1986.

[52] P. R. Prucnal. All-optical ultra-fast networks. *SPIE Proc.*, Vol. 715:42, 1986.

[53] M. A. Santoro P. Prucnal and S. K. Sehgal. Ultrafast all-optical multiple access fiber networks. *IEEE J. Select. Areas Commun.*, Vol. 4:1484, No. 8, 1986.

[54] M. A. Santoro and P. Prucnal. Asynchronous fiber optic local area network using cdma and optical correlation. *IEEE Proc.*, Vol. 75:1336, No. 9, 1987.

[55] W.C. Kwong and P.R. Prucnal. Synchronous cdma demonstration for fibreoptic networks with optical processing. *Electron. Lett.*, Vol. 26:2219, No. 24, 1990.

[56] P.R. Prucnal W.C. Kwong, P.A. Perrier. Performance comparision of asynchronous and synchronous code-division multiple access techniques for fiber-optic local area networks. *IEEE Trans. On Comm.*, Vol. 39:pp: 1625–1634, Nov. 1991.

[57] H. M. H. Shalaby. Chip-level detection in optical code-division multiple-access. *Journal of Lightwave Tech.*, Vol. 16:1077–1087, June 1998.

[58] T. Ohtsuki. Performance analysis of direct-detection dptical asynchronous cdma systems with double-optical hard-limiters. *IEICE Trans. Comm.*, Vol. E81-B, July 1998.

[59] H. M. Kwon. Optical orthogonal code-devision multiple-access system–part i: Apd noise and thermal noise. *IEEE Trans. On Comm.*, Vol. 42:pp: 2470 – 2479, July 1994.

[60] R. J. Mcyntyre. The distribution of gains in uniformly multiplying avalanche photodiods: Theory. *IEEE Trans. Electron Devices*, Vol. ED-19:pp: 703–713, June 1972.

[61] J. B. Abshire. Performance of ook and low-order ppm modulations in optical communications when using apd-based receivers. *IEEE J. Comm.*, Vol. COM-32:pp: 1140–1143, Oct. 1984.

[62] G.-C. Yang. Performance analysis for synchronization and system on CDMA optical fiber networks. *IEICE Trans. Comm.*, Vol. E77B, No. 10:pp: 1238–1248, Oct. 1994.

[63] Jawad A. Salehi Abtin Keshavarzian. Multiple-Shift Code Acquisition of Optical Orthogonal Codes in Optical CDMA systems. *IEEE Trans. Comm.*, Vol. 53, No. 4:pp: 687 – 697, April 2005.

[64] J. Bajcsy R. M. H. Yim, L. R. Chen. Design and performance of 2-D codes for wavelength-time optical CDMA. *IEEE Photon. Technol. Lett.*, Vol. 14:pp: 714–716, May 2002.

[65] L. R. Chen. Flexible fiber Bragg grating encoder/decoder for hybrid wavelength-time optical CDMA. *IEEE Photon. Technol. Lett.*, vol. 13:pp: 1233–1235, Nov. 2001.

[66] B. Jalali Yegnanarayanan, A. S. Bhushan. Fast wavelength-hopping time-spreading encoding/decoding for optical CDMA. *IEEE Photon. Technol. Lett.*, Vol. 12:pp: 573–576, May 2000.

[67] G. C. Yang, G.-C., and W.C. Kwong. Performance analysis of optical cdma with prime codes. *Electronics Letters*, Vol. 31:569–570, March 1995.

[68] R. Calvani et al. Polarization shift keying: A coherent transmission technique with differential heterodyne detection. *Electron. Lett.*, Vol. 24:pp: 642–643, May 1988.

[69] F. Delpiano G. Marone R. Calvani, R. Caponi. An experiment of optical heterodyne transmission with polarization modulation at 140 mbit/s bitrate and 1550 nm wavelength. *1991. GLOBECOM '91. Countdown to the New Millennium. Featuring a Mini-Theme on: Personal Communications Service*, 2-5 Dec 1991.

[70] W. K. Burns P. M. Hill, R. Olshansky. Optical polarization division multiplexing at 4 gb/s. *IEEE Photonics Technology Letters*, Vol. 4 , Issue: 5:pp: 500 – 502, May 1992.

[71] P. Poggiolini S. Benedetto, R. Gaudino. Direct detection of optical digital transmission based on polarization shift keying modulations. *IEEE Journal on Selected Areas in Communications*, Vol. 13 ,Issue 3:pp: 531 – 542, April 1995.

[72] C.D. Poole et al. Phenomenological approach to polarization in long single-mode fibers. *Journal of Lightwave Technology*, Vol. 22, no. 19:pp: 1029–1030, Sept. 11, 1986.

[73] L.G. Cimini et al. Preservation of polarization orthogonality through a linear optical system. *Electron. Lett.*, Vol. 23, no. 23:pp: 1365–1366, Dec. 3, 1987.

[74] C.D. Poole et al. Polarization dispersion and principal states in a 147-km undersea lightwave cable. *Journal of Lightwave Technology*, Vol. 6:pp: 1185–1190, July 1988.

[75] S. Benedetto P. Poggiolini. Theory of polarization spreading techniques-part i. *IEEE Trans. Comm.*, Vol. 42:pp: 2105, May 1994.

[76] Fred Heismann. High-speed polarization scrambler with adjustable phase chirp. *IEEE journal of selected topics in Quantum Electr.*, Vol. 2, no. 2:pp: 311, June 1996.

[77] Mario A. Santoro and Craig D. Poole. Polarization scrambling using a short piece of high-birefringence optical fiber and a multifrequency laser diode. *Journal of lightwave tech.*, Vol. 12, no. 12:pp: 288, Feb. 1994.

[78] Fred Heismann. Compact electro-optic polarization scramblers for optically amplified lightwave systems. *journal of lightwave tech.*, Vol. 14, no. 8:pp: 1801, August 1996.

[79] G. Nichlson and D. Tempe. Polarization fluctuation measurements on installed single-mode fibre. *J. lightwave Technology*, Vol. 7, Issue 8:pp: 1197–1200, 1989.

[80] P. Poggiolini S. Benedetto. Theory of polarization shift keying. *IEEE Transactions on Communications*, Vol. 40, Issue:4:pp:708 – 721, April 1992.

[81] K. Wong M. Marhic L. Kazofsky K. Shimizu E. Hu, Y. Hsueh and N. Kikuchi. 4-level direct-detection polarization shift-keying (dd-polsk) system with phase modulators. *Proc. OFC'2003, Atalanta, USA*, pages pp: 647–649, 23-28 March 2003.

[82] J. P. Gordon and H. Kogelnik. Pmd fundamentals: Polarization mode dispersion in optical fibers. *PNAS*, Vol. 97, No. 9, April 25, 2000.

[83] A. G. Weidner. The poincare sphere: Isolated and real trajectories describing the state of polarization. *Progr. Quantum Electron.*, Vol. 23, No. 1:pp: 3–12, 1992.

[84] S.V Maric; O. Moreno and C.J. Corrada. Multimedia transmission in fiber-optic lans using optical cdma. *Journal of Lightwave Tech.*, Vol. 14, Issue: 10:pp: 2149 – 2153, Oct. 1996.

[85] S.V. Maric and V.K. Lau. Multirate fiber-optic cdma: System design and performance analysis. *Journal of Lightwave Tech.*, Vol. 16, No. 1:pp: 9 – 17, January 1998.

[86] W.C. Kowng and G.-C. Yang. Double-weight signature pattern codes for multicore-fiber code-division multiple-access networks. *IEEE Comm. Lett.*, Vol. 5:pp: 203–205, May 2001.

[87] F.-R. Gu and J. Wu. Construction and performance analysis of variable-weight optical orthogonal codes for asynchronous optical cdma systems. *Journal of Lightwave Tech.*, Vol. 23, No. 2:pp: 740–748, February 2005.

[88] W.C. Kowng and G.-C. Yang. Design of multilength optical orthogonal codes for optical cdma multimedia networks. *IEEE Trans. Comm.*, Vol. 50:pp: 1258–1265, Aug. 2002.

[89] Jian-Guo Zhangg. Variable-bit-rate video transmission systems using optical fiber code-division multiplexing scheme. *IEEE Trans. Consumer Electronics*, Vol. 42:874 – 884, Nov. 1996.

[90] L. Xu I. Glesk V. Baby, B.C. Wang and P.R. Prucnal. Highly scalable serial-parallel optical delay line. *Optics Communications*, Vol. 218:pp: 235–242, April 2003.

[91] N.G. Tarhuni and T.O. Korhonen. Multi-weight multi-length strict optical orthogonal codes. *6th Nordic Signal Processing Symposium, NORSIG 2004*, Vol. 11:161–164, June 9 - 11, 2004 Espoo, Finland.

[92] T.H. Shake. Security performance of optical cdma against eavesdropping. *Journal of Lightwave Tech.*, Vol. 23, No. 2:655–670, February 2005.

[93] G. Ge and J. Yin. Constructions for optimal (v, 4, 1) optical orthogonal codes. *IEEE Trans. Inform.*, Vol. 47:pp: 2998–3004, 2001.

[94] M.B.-Pearce and B. Aazhang. Performance analysis of single-user and multiuser detectors for optical code division multiple access communication systems. *IEEE Trans. Comm.*, Vol. 43:pp: 435–444, Feb/March/April 1995.

[95] L.B. Nelson and H.V. Poor. Performance of multiuser detection for optical cdma–part i: Error probabilities. *IEEE Trans. Comm.*, Vol. 43:pp: 2803–2811, Nov. 1995.

[96] T.K. Tang and K.B. Letaief. Bit-error rate computation of optical cdma communication systems by large deviations theory. *IEEE Trans. Comm.*, Vol. 46:1422–1428, Nov. 1998.

[97] Hwei P. HSU. *Theory and Problems of Probability, Random Variables, and Random Processes*. Schaum's Outline Series, McGRAW-HILL, 1997.

[98] Howard M. Taylor and Samuel Karlin. *An Introduction to Stochastic Modeling*. Academic Press, third edition, 1998.

[99] H. Chung and P. V. Kumar. Optical orthogonal codes-new bounds and an optimal construction. *IEEE Trans. Inf. Theory*, Vol. 36:pp: 866–873, Jul. 1990.

[100] Jingshown Wu Chi-Shun Weng. Optical orthogonal codes with large crosscorrelation and their performance bound for asynchrounous optical cdma systems. *Journal of Lightwave Technology*, Vol. 19:pp 735–742, Dec. 2001.

[101] H. Yashima and T. Kobayashi. Ocdma with time-hopping and power control for multimedia networks. *Journal of Lightwave Tech.*, Vol. 21, No. 3:pp: 695, March 2003.

[102] L. A. Rusch E. Intay and P. Fortier. Multirate optical fast frequency-hopping cdma system using power control. *IEEE GLOBECOM'00*, Vol. 2:pp: 1221 – 1227, 27 Nov. - 1 Dec. 2000.

[103] P. Fortier E. Intay, H.M.H. Shalaby and L.A. Rusch. Multirate optical fast frequency-hopping cdma system using power control. *Journal of Lightwave Tech.*, Vol. 20, No. 2:166, February 2002.

[104] Mohammed S. Elmusrati. radio resource scheduler and smart antenna in cellular communication systems. *Ph.D. thesis, Control Engineering Laboratory, Helsinki University of Technology*, 2004.

[105] F. Gantmacher. *The Theory of Matrices*. Chelsea Publising Company, 1964.

[106] G.-C.; W.C. Kwong G. C. Yang. *Prime Codes with Applications to CDMA Wireless and Optical Networks*. 2002.

[107] R. Yates. A framework for uplink power control in cellular radio systems. *IEEE J. Select. Areas Commun.*, Vol. 13:pp: 1341–1347, Sep. 1995.

[108] R. Jantti. *Power control and transmission rate management in cellular radio systems*. Ph.D. thesis, Control Engineering Laboratory, Helsinki University of Technology, 2001.

Publications

HELSINKI UNIVERSITY OF TECHNOLOGY COMMUNICATIONS LABORATORY T-REPORTS

T43 Esa Malkamäki: Performance of error control over block fading channels with ARQ applications, väitöskirja, 23.10.1998, 150 s.

T44 Timo Korhonen: Measuring and estimating instantaneous radio channel by regularized deconvolution, väitöskirja, 8.10.1999, 159 s + liitteet.

T45 Pauli Lallo: Investigation of Data Transmission over an Adaptive Delta Modulated Voice Channel by Simulations Using a Spreadsheet Program, 1999, 30 s.

T46 Heikki P.S. Leivo: Tietoliikennetekniikan tulevat mahdollisuudet, Tulevaisuus-kysely II, Tutkimus 29.7.2000, 20 s.

T47 Asko Parviala: Intensity Measurements in an Analogue Local Telephone Network, Summary and Conclusion, with Applications to the Digital Networks and Data Service, 16.7.2001, 38 s.

T48 Sampo Niskanen and Patric R.J. Östergård: Cliquer User's Guide, Version 1.0 17.2.2003, pp. 26

T49 Harri Holma: A Study of UMTS Terrestrial Radio Access Performance, väitöskirja, 24.10.2003

T50 Edward Mutafungwa: Design and Performance Analysis of Pure and Hybrid WDM Optical Networks (2004), väitöskirja

T51 Martti Lagus: Physical and Experimental Basis for Telecommunications Environmental Standards 7.3.2005, 43 s.

T52 Muhammad Jahangir Hossain Sarker: Random Access Protocol and its Impacts on Air Interface in Cellular Networks (2005) väitöskirja

T53 David Soldani: QoS Management in UMTS Terrestrial Radio Access FDD Networks (2005) väitöskirja

T54 Markku Liinaharja: Studies on the Performance of Some ARQ Schemes (2006) väitöskirja

T55 Abdulla Ali Abouda: Characterization of MIMO Channel Capacity in Urban Microcellular Environment (2007) väitöskirja

ISBN 978-951-22-8723-9
ISSN 0356-5087